

Metal ion binding to iron oxides

M. Ponthieu^{a,d}, F. Juillot^b, T. Hiemstra^c, W.H. van Riemsdijk^c, M.F. Benedetti^{d,*}

^a *Laboratoire de Géochimie et Métallogénie, Université Pierre and Marie Curie, UMR CNRS 7047, 4 Place Jussieu, 75252 Paris Cedex 05, France*

^b *Laboratoire de Minéralogie-Cristallographie, Universités Pierre and Marie Curie et Denis Diderot, UMR CNRS 7590, 4 Place Jussieu, 75252 Paris Cedex 05, France*

^c *Wageningen University, Sub-department of Soil Quality, Postbus 8005, 6700 EC Wageningen, The Netherlands*

^d *Laboratoire de Géochimie des Eaux, Université Denis Diderot, IPGP, case 7052 2 Place Jussieu, 75251 Paris Cedex 05, France*

Received 12 April 2005; accepted in revised form 14 February 2006

Abstract

The biogeochemistry of trace elements (TE) is largely dependent upon their interaction with heterogeneous ligands including metal oxides and hydrous oxides of iron. The modeling of TE interactions with iron oxides has been pursued using a variety of chemical models. The objective of this work is to show that it is possible to model the adsorption of protons and TE on a crystallized oxide (i.e., goethite) and on an amorphous oxide (HFO) in an identical way. Here, we use the CD-MUSIC approach in combination with valuable and reliable surface spectroscopy information about the nature of surface complexes of the TE. The other objective of this work is to obtain generic parameters to describe the binding of the following elements (Cd, Co, Cu, Ni, Pb, and Zn) onto both iron oxides for the CD-MUSIC approach. The results show that a consistent description of proton and metal ion binding is possible for goethite and HFO with the same set of model parameters. In general a good prediction of almost all the collected experimental data sets corresponding to metal ion binding to HFO is obtained. Moreover, dominant surface species are in agreement with the recently published surface complexes derived from X-ray absorption spectroscopy (XAS) data. Until more detailed information on the structure of the two iron oxides is available, the present option seems a reasonable approximation and can be used to describe complex geochemical systems. To improve our understanding and modeling of multi-component systems we need more data obtained at much lower metal ion to iron oxide ratios in order to be able to account eventually for sites that are not always characterized in spectroscopic studies.

© 2006 Elsevier Inc. All rights reserved.

1. Introduction

The biogeochemical cycling of trace elements (TE) in soil and aquatic environments is increasingly affected by anthropogenic activities. The perturbation of biogeochemical cycles by mankind occurs at nano, micro, and macro scales. A major objective of geochemistry is to characterize these changes and to forecast the response of natural systems to human perturbations. The mobility and the bioavailability of TE in aquatic systems, soils, and sediments are largely dependent upon their interaction with organic ligands such as humic substances (Tipping, 1998;

Kinniburgh et al., 1999) and/or mineral surfaces like clays, metal oxides, and hydrous oxides of aluminium, iron, and manganese (Stumm and Morgan, 1981).

Iron oxides (i.e., hematite, goethite, hydrous ferric oxide (HFO), etc.) are common minerals in soils and colloids in aquatic environments (Buffle, 1990). The sorption of TE by these oxides is important since it will significantly control their concentration and speciation in complex geochemical systems. Moreover the availability of nutrients and the mobility of toxic TE to living organisms will also depend on the nature and the strength of the interactions with the oxide surfaces.

The modeling of TE interactions with iron oxides in aquatic and soil systems can be pursued using a variety of chemical models. Since the early work of Stumm and colleagues (Schindler and Kamber, 1968; Stumm et al.,

* Corresponding author. Fax: +33 1 44 27 60 38.

E-mail address: benedetti@ipgp.jussieu.fr (M.F. Benedetti).

1970; Huang and Stumm, 1973) numerous variations have been developed (Davies and Leckie, 1979; Van Riemsdijk et al., 1986; Westall, 1986; Dzombak and Morel, 1990). More recently, new approaches have been proposed. For instance, Sverjenski and Sahai (1996) and Crescenti and Sverjenski (1999) combine an Extended Triple Layer Model with a 2 pK approach for one surface site while a new multisite approach has been developed to account for the chemical heterogeneity of oxide surfaces (Hiemstra et al., 1989a,b). A comparison of the performance of the most commonly used surface complexation models can be found in Venema et al. (1996a).

A limitation of some of the above mentioned models is that the crystallographic nature of the reactive sites is not always taken into account. Recent advances in surface spectroscopy (Brown et al., 1999 and references therein) have generated numerous valuable and reliable information about the nature of surface complexes of TE that can be incorporated in Surface Complexation Modeling (SCM).

Application of any of these models to complex multi-component systems requires a set of suitable parameters to describe the binding characteristics of the individual TE. Explicit measurement of these binding properties is difficult. For this reason, standardization of SCM approaches has been proposed for HFOs (Dzombak and Morel, 1990). These authors have suggested that a model should involve a minimum number of adjustable parameters. The availability of a robust and extensive set of parameters for a given model is therefore highly desirable. Macroscopic data (not shown here) obtained with the same surface loading (i.e., sorption edge experiments) show that goethite and HFO have comparable pH sorption edges for Pb, Cu, and Cd (sorption edges from: Benjamin, 1978; Leckie et al., 1980; Benjamin and Bloom, 1981; Benjamin and Leckie, 1981 for HFO and from: Balistrieri and Murray, 1982; Johnson, 1990; Kooner, 1992 for goethite). Conversely, Zn sorption edges for the two oxides are different.

Most recent molecular scale observations highlighted by XAS also show similarities for Cd, Cu, and Pb binding to HFO and goethite. Spadini et al. (1994) reported that the crystallographic sites involved in cadmium complexation are similar on goethite and on HFO. Trivedi et al. (2003) suggested that adsorbed Pb could have similar coordination environments for these two mineral phases. On the other hand, Waychunas et al. (2002) showed that Zn adsorbed on goethite and on HFO has a different geometry. This latter finding could explain the difference in the adsorption curves reported earlier and the different behavior of Zn with respect to Cd, Cu, and Pb.

Several publications present CD-MUSIC applications on experimental data (Venema et al., 1996a; Boily et al., 2000; Rietra et al., 2001). Weng et al. (2001) used this approach to calculate trace element (Cu, Cd, Zn, Pb, and Ni) speciation in a soil and estimate the amount of TE adsorbed onto goethite. However, they used a different approach to estimate the amount of metal ions bound to

HFO. This was done using the generic parameters proposed in the Dzombak and Morel (1990) approach.

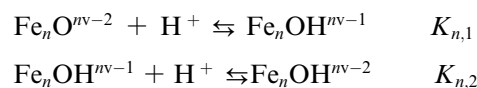
Based on previous macroscopic and microscopic observations (see above), this study demonstrates that the same approach for the two iron oxides can be used to account for their reactivity towards protons and a large number of TE. This is especially relevant for the modeling of complex natural or human impacted geochemical systems. Rather than considering two distinct ferric oxides, we can then consider only one kind of particle that combines the properties of crystallized and amorphous iron oxides. This approach results in a smaller number of adjustable parameters. Moreover, for field systems, several chemical protocols are available to estimate the respective amounts of crystallized and amorphous iron oxides in soils and sediments (Schwertmann and Cornell, 1991). Once the respective proportion of the two types of iron oxides is known, it is incorporated in the modeling by converting the respective mass of the two types of oxides into surface areas and site densities as described in greater detail below.

The first objective of this work is to show that it is possible to model the adsorption of protons and TE on a crystallized iron oxide (i.e., goethite) and on an amorphous iron oxide (HFO) in an identical way using the CD-MUSIC approach. The CD-MUSIC approach applied to complex field systems, like in the work of Weng et al. (2001), requires a set of generic parameters (i.e., parameters that can be used regardless of the experimental conditions) for a series of TE. The other objective of this work is to obtain generic parameters able to describe the binding of the following elements (Co, Ni, Cu, Zn, Cd, and Pb) onto both crystalline and amorphous iron oxides. A compilation of an extended database of TE interactions with both iron oxides will be made to derive the generic parameters.

2. Methods

2.1. The CD-MUSIC model (Hiemstra and Van Riemsdijk, 1996)

The iron oxide surface is heterogeneous because of several surface groups having different reactivities (Venema et al., 1998). The description of iron oxide surface charging behavior is made with a complexation model including sites which protonate in two steps:



where n is the number of the underlying iron ions and ν is the bond valence that follows from the Pauling's principle of charge distribution defined as the charge of the central ion (i.e., +3 for Fe(III)) divided by the number of surrounding ligands (i.e., 6 for Fe(III) in octahedral coordination geometry). It was shown that $\log K_H$ of both consecutive reactions differs strongly (Hiemstra et al., 1989b). This implies that only one of the two steps is of rel-

evance for the charging behavior in natural systems (Hiemstra et al., 1989b).

In CD-MUSIC, the charge of an adsorbed ion is divided between the ligands present at the surface plane and those present in an intermediate plane. The charge distribution (f) can be used as a fitting parameter or derived from the exact structure of the surface complex as measured by EXAFS.

2.2. Model parameters

In this section, we will describe the various assumptions made to simulate the experimental database assembled. In the first part we will refer mostly to assumptions made on the oxides structure, the specific surface areas of the major crystallographic planes ([110], [021]) and to parameters like proton affinities, capacitance of the different layers, and ion pair formation constants used to describe the proton binding behavior. In the last part, the choices of TE surface complexes are discussed and the TE binding constants and charge distribution parameters are defined.

2.2.1. Oxides structure: Goethite and HFO

The structure of goethite consists of double chains of Fe octahedral cross-linked by corner linkages. The dominant crystal planes of goethite are the [110] and the [021] (Schwertmann and Cornell, 1991). It has been shown that the [110] plane running parallel to the long axis of the laths is dominant (i.e., 80–95% of the total surface area). The chain terminations are bounded by the much smaller [021] plane (Schwertmann and Cornell, 1991). Because of its needle-shape, goethite has a high proportion of low affinity sites located along its chain length and a low proportion of high affinity sites located in the [021] planes. The specific surface area of goethite varies between 30 and 100 m² g⁻¹. In the goethite structure, the oxygen can be singly (FeO), doubly (Fe₂O) or triply (Fe₃O) coordinated. Two types of oxygen can be distinguished in the goethite structure, unprotonated oxygen (O_{II}) and protonated oxygen (O_I) (Venema et al., 1998).

Manceau and Combes (1988), Manceau and Charlet (1994), and Spadini et al. (1994) have pointed out the similarity between goethite and HFO local structure. Their structures differ by their medium and long-range order, HFO having shorter octahedral chains. The extreme shortening of octahedral chains results in a tremendous increase in the amount of high affinity sites. The specific surface area of HFO is much higher than that of the goethite and varies between 200 and 800 m² g⁻¹ depending strongly on the measurement procedure (Dzombak and Morel, 1990).

The two dominant crystal planes ([110] and [021]) are treated as having their own electrostatic potential and double layer. This is the first time that such an approach for goethite or HFO has been advanced. Previously, only an averaged simplified composition was used with one electrostatic plane (Venema et al., 1996a,b). By giving each plane its own electrostatic potential, it becomes very easy to ap-

ply the approach based on the use of a unique particle combining the properties of the two oxides.

2.2.2. Proton affinities, sites density, and capacitance

We use, in this work, the detailed predicted proton affinity constants instead of the much more simplified approach used in the past. Hiemstra and Van Riemsdijk (1996) and Hiemstra et al. (1996) found a linear relationship between the log K_H values and the actual oxygen charge:

$$\log K_H = -19.8 \left(-2 + ms_H + n(1 - s_H) + \sum_i^{n_{st}} s_{i,st} \right), \quad (1)$$

where m is the number of donating H-bridges with adsorbed water, n the number of accepting H-bridges with adsorbed water, n_{st} the total number of structural bonds, s_i the bond valence of a structural Me–O or H–O bond and s_H the bond valence for an adsorbed proton ($s_H = 0.8$) (Hiemstra and Van Riemsdijk, 1996 and Hiemstra et al., 1996). The log K_H value is directly related to the actual bond valence, s_{i-j} , and then to the bond length between two elements, according to the following expression for s_{i-j} :

$$s_{i-j} = e^{(R_{i-j} - R_{0,i-j})/0.37}, \quad (2)$$

where R_{i-j} is the bond length, $R_{0,i-j}$ is an ion dependent parameter ($R_{0,Fe-O} = 1.759$, value optimized for a broad range of environments) (Hiemstra and Van Riemsdijk, 1996 and Hiemstra et al., 1996), and the value of 0.37 is found empirically by Brown and Altermatt (1985) as the best parameter for different types of bonds.

As mentioned before, two types of oxygen are distinguished in the goethite structure (O_I and O_{II}). In the calculations, a distinction is made between internal H-bridges of a surface ligand (noted O_I) and H-bridges between a surface ligand and adsorbed water (noted OH). Internal H-bridges are part of the crystal structure and do not contribute to the value of $n + m$ in Eq. (1) above.

Venema et al. (1998) calculated the log K_H values for the different surface groups using Eq. (1), as well as the total number of reactive groups from crystallographic data (i.e., site densities in Appendix A). The pair formation constants (K_i) values for Na⁺ and NO₃⁻ are taken from Hiemstra and Van Riemsdijk (1996).

The capacitance values are optimized using the different parameters defined by Hiemstra and Van Riemsdijk (1996) and Venema et al. (1998) (log K_H , log K_i , and site density) to simulate the charging curves of goethite for three electrolyte levels taken from Venema et al. (1998), and the same values of the capacitance and of the ion pair formation constants are used for the two crystal planes ([110] and [021]).

2.2.3. Surface complexes

Different kind of linkages are involved in the formation of the surface complexes: apices, corners, edges or faces. Each type of linkage results in a discrete and characteristic

Me–Fe distance. EXAFS spectroscopy can be used to discriminate between these different mechanisms of attachment.

2.2.3.1. Cadmium. The cadmium is considered to have a six-fold coordination, i.e., forming an octahedron with oxygen atoms (O, OH, OH₂) (Spadini et al., 1994; Randall et al., 1999). Two different cadmium–iron distances are reported by Spadini et al. (1994) and interpreted as two different surface complex structures: edge-linkage and corner-linkage. They proposed two types of complexes for each goethite plane: on the [110] plane, monodentate complexes with doubly coordinated oxygen (sharing a single corner) and bidentate complexes with singly coordinated oxygen (sharing a double corner); on the [021] plane, a tridentate complex with two singly coordinated and one doubly coordinated surface group sharing two edges and another tridentate complex with two singly coordinated and one doubly coordinated surface group sharing one edge and two corners. Spadini et al. (1994) found that the relative abundance of surface complexes having an edge-linkage decreases with increasing cadmium surface loading and concluded that surface complexes having an edge-linkage have a higher cadmium affinity than surface complexes with only a corner-linkage. Randall et al. (1999) reported only one cadmium–iron distance which they interpreted as a

double corner-linkage. They did not observe the sharing edge complexes located on [021] plane. This is not surprising since in their experiments this plane only represents 2% of the total surface area, which was likely too small to be observed in their EXAFS measurements relative to the dominant corner-sharing complexes located on [110] plane.

In agreement with these studies, and considering the results of Venema et al. (1996b) suggesting that singly coordinated surface groups are the most important reactive surface groups for specific adsorption, we have chosen bidentate complexes for the [110] plane (Table 1). For the [021] plane, complexes involving two edges were chosen. This configuration has the highest affinity for cadmium (Venema et al., 1996b) (Table 1). This complex combines three surface groups: FeO_IH, FeO_{II}H, and Fe₂O_IH. However, in the actual version of the speciation code (ECOSAT, Keizer and Van Riemsdijk, 1999) only the combination of two surface groups is possible. Instead of FeO_IH and FeO_{II}H, we will use a combination of both groups, named FeOH_m for the modeling of the adsorption experiments. For the modeling of the charging curves, we used the two distinct groups. Nonetheless calculations were done using the 2 distinct groups (FeO_IH and FeO_{II}H) and the 2 ‘mean’ groups (FeOH_m) and the results are quite similar (difference smaller than 15%) for the pH values below

Table 1
Surface complexes selected from the literature for the fitting of macroscopic experimental data sets given in Appendix B and C with the CD-MUSIC approach

		Complexes		References
Cd	[110] Plane	$[(\equiv\text{Fe}-\text{O}_{\text{II}}\text{H})_2-\text{Cd}]^+$ $[(\equiv\text{Fe}-\text{O}_{\text{II}}\text{H})_2-\text{CdOH}]^0$	$K_{\text{Cd-1}}$ $K_{\text{CdOH-1}}$	Spadini et al. (1994)
	[021] Plane	$[(\equiv\text{Fe}-\text{OH}_m)_2-\text{Cd}-(\text{HO}_I-\text{Fe}_2\equiv)]^+$ $[(\equiv\text{Fe}-\text{OH}_m)_2-\text{CdOH}-(\text{HO}_I-\text{Fe}_2\equiv)]^0$	$K_{\text{Cd-3}}$ $K_{\text{CdOH-3}}$	Venema et al. (1996b)
Cu	[110] Plane	$[(\equiv\text{Fe}_2-\text{O}_{\text{II}}\text{H})_2-\text{Cu}]^{2+}$ $[(\equiv\text{Fe}_2-\text{O}_{\text{II}}\text{H})_2-\text{CuOH}]^+$	$K_{\text{Cu-1}}$ $K_{\text{CuOH-1}}$	Alcacio et al. (2001) Parkman et al. (1999)
		$[(\equiv\text{Fe}-\text{O}_{\text{II}}\text{H})_2-\text{Cu}-(\text{O}_I-\text{Fe}_3\equiv)]^{+1/2}$ $[(\equiv\text{Fe}-\text{O}_{\text{II}}\text{H})_2-\text{CuOH}-(\text{O}_I-\text{Fe}_3\equiv)]^{-1/2}$	$K_{\text{Cu-2}}$ $K_{\text{CuOH-2}}$	Bochatay et al. (1997)
	[021] Plane	$[(\equiv\text{Fe}-\text{OH}_m)_2-\text{Cu}-(\text{HO}_I-\text{Fe}_2\equiv)]^+$ $[(\equiv\text{Fe}-\text{OH}_m)_2-\text{CuOH}-(\text{HO}_I-\text{Fe}_2\equiv)]^0$	$K_{\text{Cu-3}}$ $K_{\text{CuOH-3}}$	
Pb	[110] Plane	$[(\equiv\text{Fe}-\text{O}_{\text{II}}\text{H})_2-\text{Pb}]^{+1}$ $[(\equiv\text{Fe}-\text{O}_{\text{II}}\text{H})_2-\text{PbOH}]^0$ $[(\equiv\text{Fe}-\text{O}_{\text{II}}\text{H})_2-\text{Pb}-(\text{O}_I-\text{Fe}_3\equiv)]^{+1/2}$ $[(\equiv\text{Fe}-\text{O}_{\text{II}}\text{H})_2-\text{PbOH}-(\text{O}_I-\text{Fe}_3\equiv)]^{-1/2}$	$K_{\text{PbOH-1}}$ $K_{\text{PbOH-1}}$ $K_{\text{Pb-2}}$ $K_{\text{PbOH-2}}$	Ostergren et al. (2000)
	[021] Plane	$[(\equiv\text{Fe}-\text{OH}_m)_2-\text{Pb}-(\text{HO}_I-\text{Fe}_2\equiv)]^+$ $[(\equiv\text{Fe}-\text{OH}_m)_2-\text{PbOH}-(\text{HO}_I-\text{Fe}_2\equiv)]^0$	$K_{\text{Pb-3}}$ $K_{\text{PbOH-3}}$	
Zn-goethite	[110] Plane	$[(\equiv\text{Fe}_2-\text{O}_{\text{II}}\text{H})_2-\text{Zn}]^{2+}$ $[(\equiv\text{Fe}_2-\text{O}_{\text{II}}\text{H})_2-\text{ZnOH}]^+$	$K_{\text{Zn-1}}$ $K_{\text{ZnOH-1}}$	Juillot et al. (2003)
	[021] Plane	$[(\equiv\text{Fe}-\text{OH}_m)_2-\text{Zn}-(\text{HO}_I-\text{Fe}_2\equiv)]^+$ $[(\equiv\text{Fe}-\text{OH}_m)_2-\text{ZnOH}-(\text{HO}_I-\text{Fe}_2\equiv)]^0$	$K_{\text{Zn-3}}$ $K_{\text{ZnOH-3}}$	Schlegel et al. (1997)
Zn-ferrihydrite	[110] Plane	$[(\equiv\text{Fe}-\text{O}_{\text{II}}\text{H})_2-\text{Zn}]^+$ $[(\equiv\text{Fe}-\text{O}_{\text{II}}\text{H})_2-\text{ZnOH}]^0$	$K_{\text{Zn-1}}$ $K_{\text{ZnOH-1}}$	Juillot et al. (2003)
	[021] Plane	$[(\equiv\text{Fe}-\text{OH}_m)_2-\text{Zn}]^+$ $[(\equiv\text{Fe}-\text{OH}_m)_2-\text{ZnOH}]^0$	$K_{\text{Zn-3}}$ $K_{\text{ZnOH-3}}$	Waychunas et al. (2002)

9. For the lowest charge density values, around the PZC values, the differences can be higher.

2.2.3.2. Copper. The copper presents a sixfold coordination on goethite, in a Jahn–Teller distorted environment with four close O atoms and two more distant O atoms (Bochatay et al., 1997; Parkman et al., 1999; Alcacio et al., 2001). Bochatay et al. (1997) studied copper complexation on goethite by XAFS. They performed adsorption experiments at pH 5 and pH 8. At pH 5, no 2nd coordination shell was detected. Conversely, at pH 8 a well-defined 2nd coordination shell was evidenced, in agreement with Parkman et al. (1999). However, none of these studies could conclusively identify the 2nd neighbor atom (i.e., Cu or Fe). Alcacio et al. (2001) performed Cu sorption experiments onto goethite between pH 4.7 and 7.9. These authors discounted the formation of Cu-hydroxy clusters or Cu surface precipitates on goethite and explained the 2nd coordination shell by an edge-sharing complex with single iron sites. According to these EXAFS observations, the copper forms edge-sharing complexes at the goethite surface. Long distances characteristic of corner-sharing complexes have not been pointed out. Recently, in a study of Cu sorption onto goethite, Peacock and Sherman (2004) gave a different interpretation. They proposed that a dimer adsorbed copper species could be found in some cases. We did not consider this surface species because, according to these authors, a bidentate corner-sharing complex could also explain the EXAFS data.

For the modeling, we will consider a bidentate edge-sharing complex involving two Fe₂OH groups for the [1 1 0] plane. Due to the lack of information about the nature of complexes formed on the [0 2 1] plane, we will consider the same complexes as for cadmium, since these two elements occur under the same octahedral geometry on goethite (Table 1).

2.2.3.3. Lead. EXAFS-based investigations have proposed either a square (Weesner and Bleam, 1998; Manceau et al., 2000) or a trigonal (Bargar et al., 1997; Ostergren et al., 2000) pyramid coordination for lead adsorbed onto goethite. Bargar et al. (1997) studied lead adsorption onto goethite between pH 6 and 8 using XAS and observed only one Pb–Fe distance around 3.30 Å interpreted as edge-sharing complexes. Ostergren et al. (2000) also used XAS to investigate lead–goethite interactions between pH 5 and 7. Like Bargar et al. (1997), they reported one short Pb–Fe distance attributed to edge-sharing complexes, at pH 7. However, for acidic experiments (pH 5), they observed two distances corresponding to corner-sharing and edge-sharing complexes. They developed a Pb sorption model onto goethite that integrates spectroscopic information with energetic and steric constraints imposed by the surface structure. They performed a site analysis for Pb binding to goethite that uses bond valence and structural considerations to constrain the interpretation of EXAFS results. They defined six possible bonding geometries for Pb on goethite (numbered 1 to 6) consistent with EXAFS

observations, by considering that the dominant first-shell coordination is a trigonal pyramid with three oxygens as nearest neighbors. Three of these six possible bonding geometries are (1) a bidentate double corner-sharing complex involving two FeOH groups, (2) a bidentate edge-sharing complex with two Fe₂OH groups, and (3) a tridentate edge-sharing complex with two FeOH and one Fe₃O groups for the [1 1 0] face. The three remaining bonding geometries are (4) a bidentate double corner-sharing complex with two FeOH groups, (5) a bidentate edge-sharing complex with a FeOH group and a Fe₂OH group, and (6) a tridentate edge-sharing complex involving two FeOH and one Fe₂OH groups for the [0 2 1] face.

Considering all these complexes would result in too many parameters for the model. Moreover, some of these complexes may only be relevant for the given set of specific experimental conditions of Ostergren et al. (2000). Since these authors observed two major distances attributed to edge-sharing and corner-sharing complexes, we will consider these two bonding geometries in the model. According to Ostergren et al. (2000), the steric limitations for the bidentate double corner-sharing site are expected to be more severe on the [0 2 1] plane than on the [1 1 0] plane. Consequently, only the first complex will be considered (Table 1). It is more difficult, based on the results of Ostergren et al. (2000), to discriminate between the two possible edge-sharing complexes. For the [1 1 0] face, we prefer the tridentate complex, this complex is more stable than the bidentate one because it involves two shared edges. For the [0 2 1] face, we will consider only one edge-sharing complex. Since the modeling of the available data is not sensitive enough to the choice of bidentate or tridentate complexes, we will use the tridentate complex for the same reason as for the [1 1 0] face (Table 1).

2.2.3.4. Zinc, a special case. Zinc does not have the same geometry when adsorbed on goethite and HFO surfaces. It can have a sixfold coordination geometry when adsorbed on goethite (Schlegel et al., 1997; Manceau et al., 2000; Juillot et al., 2003) and a fourfold one when sorbed on HFO (Waychunas et al., 2002; Juillot et al., 2003).

For goethite, Schlegel et al. (1997) and Juillot et al. (2003) observed by EXAFS two distinct Zn–Fe distances (3.10 and 3.30 Å) both consistent with edge-sharing complexes. For the [1 1 0] face, we will then consider bidentate edge-sharing complexes involving two Fe₂OH groups. For the [0 2 1] face, we do not have enough information to conclude on the exact nature of the complexes formed and we will consider complexes similar to those used for Cd and Cu (Table 1).

For HFO, a single Zn–Fe contribution is observed at 3.45 Å, suggesting double corner-sharing complexes (Waychunas et al., 2002; Juillot et al., 2003). Consequently, we will consider bidentate double corner-sharing complexes involving two FeOH groups for the [1 1 0] and [0 2 1] faces (Table 1).

2.2.4. Metal affinities and charge distribution

To adjust the complexation constant ($\log K_{Me}$) and the charge distribution (z_0 = charge located at the surface

Table 2

Surface complexes and median metal binding constants (± 2 standard deviations) and charge distribution used to describe metal adsorption on ferric oxides (goethite and HFO) with the CD-MUSIC approach.

		Complexes	$\log K_{Me}$	z_0/z_1
Cd	[110] Plane	$[(\equiv\text{Fe}-\text{O}_{11}\text{H})_2-\text{Cd}]^+$ $[(\equiv\text{Fe}-\text{O}_{11}\text{H})_2-\text{CdOH}]^0$	$\log K_{\text{Cd}-1} = 7 (\pm 0.9)$ $\log K_{\text{CdOH}-1} = 12 (\pm 1)$	1.05/0.95
	[021] Plane	$[(\equiv\text{Fe}-\text{OH}_m)_2-\text{Cd}-(\text{HO}_1-\text{Fe}_2\equiv)]^+$ $[(\equiv\text{Fe}-\text{OH}_m)_2-\text{CdOH}-(\text{HO}_1-\text{Fe}_2\equiv)]^0$	$\log K_{\text{Cd}-3} = 11.5 (\pm 0.6)$ $\log K_{\text{CdOH}-3} = 14.5 (\pm 0.9)$	1.05/0.95
Pb	[110] Plane	$[(\equiv\text{Fe}-\text{O}_{11}\text{H})_2-\text{Pb}]^{+1}$ $[(\equiv\text{Fe}-\text{O}_{11}\text{H})_2-\text{PbOH}]^0$ $[(\equiv\text{Fe}-\text{O}_{11}\text{H})_2-\text{Pb}-(\text{O}_1-\text{Fe}_3\equiv)]^{+1/2}$ $[(\equiv\text{Fe}-\text{O}_{11}\text{H})_2-\text{PbOH}-(\text{O}_1-\text{Fe}_3\equiv)]^{-1/2}$	$\log K_{\text{PbOH}-1} = 8.6 (\pm 0.8)$ $\log K_{\text{PbOH}-1} = 15.5 (\pm 1)$ $\log K_{\text{Pb}-2} = 11.5 (\pm 0.6)$ $\log K_{\text{PbOH}-2} = 17.8 (\pm 0.6)$	1/1 1.1/0.9
	[021] Plane	$[(\equiv\text{Fe}-\text{OH}_m)_2-\text{Pb}-(\text{HO}_1-\text{Fe}_2\equiv)]^+$ $[(\equiv\text{Fe}-\text{OH}_m)_2-\text{PbOH}-(\text{HO}_1-\text{Fe}_2\equiv)]^0$	$\log K_{\text{Pb}-3} = 15.5 (\pm 1)$ $\log K_{\text{PbOH}-3} = 19.5 (\pm 0.7)$	1.1/0.9
Cu	[110] Plane	$[(\equiv\text{Fe}_2-\text{O}_{11}\text{H})_2-\text{Cu}]^{2+}$ $[(\equiv\text{Fe}_2-\text{O}_{11}\text{H})_2-\text{CuOH}]^+$ $[(\equiv\text{Fe}-\text{O}_{11}\text{H})_2-\text{Cu}-(\text{O}_1-\text{Fe}_3\equiv)]^{+1/2}$ $[(\equiv\text{Fe}-\text{O}_{11}\text{H})_2-\text{CuOH}-(\text{O}_1-\text{Fe}_3\equiv)]^{-1/2}$	$\log K_{\text{Cu}-1} = 8.5 (\pm 0.8)$ $\log K_{\text{CuOH}-1} = 15.5 (\pm 0.8)$ $\log K_{\text{Cu}-2} = 12 (\pm 0.4)$ $\log K_{\text{CuOH}-2} = 18.8 (\pm 1.2)$	1.1/0.9 1.2/0.8
	[021] Plane	$[(\equiv\text{Fe}-\text{OH}_m)_2-\text{Cu}-(\text{HO}_1-\text{Fe}_2\equiv)]^+$ $[(\equiv\text{Fe}-\text{OH}_m)_2-\text{CuOH}-(\text{HO}_1-\text{Fe}_2\equiv)]^0$	$\log K_{\text{Cu}-3} = 13.2 (*)$ $\log K_{\text{CuOH}-3} = 19.2 (*)$	1.2/0.8
Zn-goethite	[110] Plane	$[(\equiv\text{Fe}_2-\text{O}_{11}\text{H})_2-\text{Zn}]^{2+}$ $[(\equiv\text{Fe}_2-\text{O}_{11}\text{H})_2-\text{ZnOH}]^+$	$\log K_{\text{Zn}-1} = 7 (\pm 0.6)$ $\log K_{\text{ZnOH}-1} = 13.8 (\pm 0.8)$	0.7/1.3
	[021] Plane	$[(\equiv\text{Fe}-\text{OH}_m)_2-\text{Zn}-(\text{HO}_1-\text{Fe}_2\equiv)]^+$ $[(\equiv\text{Fe}-\text{OH}_m)_2-\text{ZnOH}-(\text{HO}_1-\text{Fe}_2\equiv)]^0$	$\log K_{\text{Zn}-3} = 12.5 (\pm 0.5)$ $\log K_{\text{ZnOH}-3} = 18 (\pm 0.8)$	0.9/1.1
Zn-ferrihydrate	[110] Plane	$[(\equiv\text{Fe}-\text{O}_{11}\text{H})_2-\text{Zn}]^+$ $[(\equiv\text{Fe}-\text{O}_{11}\text{H})_2-\text{ZnOH}]^0$	$\log K_{\text{Zn}-1} = 7.2 (\pm 0.4)$ $\log K_{\text{ZnOH}-1} = 13.9 (\pm 0.4)$	0.9/1.1
	[021] Plane	$[(\equiv\text{Fe}-\text{OH}_m)_2-\text{Zn}]^+$ $[(\equiv\text{Fe}-\text{OH}_m)_2-\text{ZnOH}]^0$	$\log K_{\text{Zn}-3} = 9.5 (\pm 0.4)$ $\log K_{\text{ZnOH}-3} = 15.8 (\pm 0.4)$	0.9/1.1

*, no standard deviation, the same constant is used to describe the different experiments.

plane, z_1 = charge located in the mid plane) for Cd, Cu, Pb, and Zn, experimental data sets from the literature were used (Appendix B). They were chosen to cover a wide range of ionic strength and different metal to goethite ratios (i.e., surface coverage). The goethite specific surface area used for the calculation is the one given by each author, but the fraction of the total area attributed to the [110] and the [021] faces is an adjustable parameter. The adjusted values are given for each experiment in Appendix C. Optimal values for the surface complexation constant and charge distribution are first determined for each metal sorption data set. Then median values of the binding constant and the charge distribution are calculated using all the optimized values. The variability of these median values is calculated as two times the standard deviation, and these values are given in Table 2.

2.2.5. From goethite to HFO

The objective of this work is to model the adsorption of protons and metal ions on a crystallized iron oxide (goethite) and on an amorphous one (HFO) in an identical way. The main difference between these two oxides is the length of their octahedral chains and hence their site densities with a higher proportion of high affinity sites present

on the HFO surface (Manceau and Combes, 1988; Manceau and Charlet, 1994; Spadini et al., 1994). These differences are considered in the model by adjusting the respective proportions of the two faces of HFO (i.e., [110] and [021]), as well as the capacitance value of the two layers and the pair formation constant. In a first step, we optimized these parameters using two HFO charging curves taken from Davies (1977) and Hsi and Langmuir (1985) using the different surface groups and associated proton affinity and site density values defined by Venema et al. (1998) for goethite. In a second step, the metal ion parameters ($\log K_{Me}$, z_0/z_1) obtained by fitting metal binding onto goethite were used without any adjustment, to predict the interactions of the metal ions with HFO. This was performed using part of the experimental database compiled by Dzombak and Morel (1990).

3. Results

3.1. Proton adsorption

3.1.1. Goethite

The pair formation constants for Na^+ and NO_3^- are fixed at $\log K_i = -1 \pm 0.5$ (Hiemstra and Van Riemsdijk,

1996). The overall capacitance C_{tot} is defined as: $C_{\text{tot}} = (C_1 \times C_2) / (C_1 + C_2)$ in which C_1 and C_2 are the capacitance of the inner and the outer layers, respectively. C_2 is set at 5 F m^{-2} according to Venema et al. (1996b) and C_1 is adjusted. The capacitance value is optimized with the charging curve data from Venema et al. (1996b) (Fig. 1). For a good description of the data, C_1 is 1.65 F m^{-2} , which gives an overall capacitance of 1.24 F m^{-2} .

Below the point of zero charge (pzc) the model fits are in good agreement with the experimental data. The calculated pzc value is equal to 9.3 and is in agreement with the measured value. The fit of the data for pH values above this pzc are less accurate.

3.1.2. HFO

The respective proportions of the two major crystallographic planes ([110] and [021]), the capacitance and the ion pair formation constant values were adjusted to describe the charging curve data. Two distinct sets of data have been used for the optimization. They are shown together with model fits in Fig. 2. The [021] plane becomes dominant and represents 63% of the total specific surface area fixed assuming that $S_{\text{tot}} = 800 \text{ m}^2 \text{ g}^{-1}$ (i.e., $S_{[110]} = 300 \text{ m}^2 \text{ g}^{-1}$ and $S_{[021]} = 500 \text{ m}^2 \text{ g}^{-1}$). The overall capacitance value is equal to 1.27 F m^{-2} with $C_1 = 1.7 \text{ F m}^{-2}$ and $C_2 = 5 \text{ F m}^{-2}$ and the ion pair formation constant $\log K_i$ is equal to -1.5 . These fitted values allow a good description of the charging curves, especially for the Hsi and Langmuir (1985) data (Fig. 2B) below the pzc. As for goethite, the fit is poor above the pzc. The calculated pzc value (i.e., pzc = 8.5–8.8) is higher than the value measured (pzc = 8). This difference may be related to the difficulties associated with performing titrations on HFO. For example, carbonate ions are difficult to remove and will interfere with the determination of the pzc (Gaboriaud and Ehrhardt, 2003), and Smith and Ferris (2001) pointed out that HFO structure is sensitive to the preparation protocol.

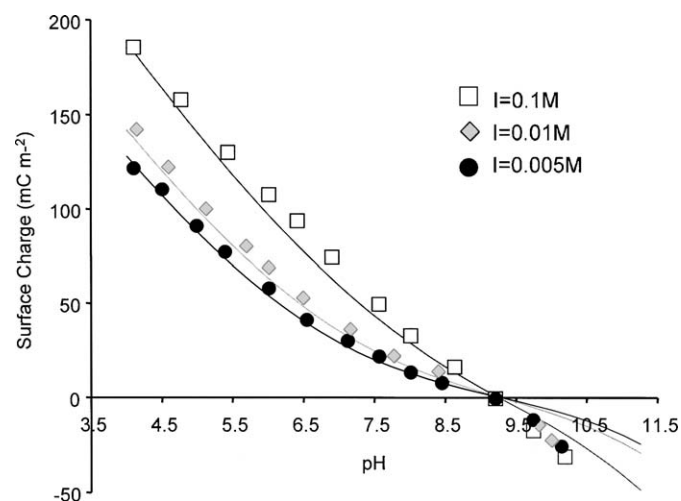


Fig. 1. Charging behavior of goethite at three different salt concentrations (data from Venema et al., 1996b). The lines correspond to model calculation using a total capacitance of $C_{\text{tot}} = 1.24 \text{ F m}^{-2}$.

3.2. Metal adsorption

The overall optimization procedure to obtain the median parameters is similar to the one used by Milne et al. (2003) for metal binding to humic substances. The optimization of the parameters related to the metal ion binding on the different binding sites ($\log K_{\text{Me}}$, z_0/z_1) was first done with various adsorption experiments of metal ions onto goethite taken from the literature (Appendix B). In a second step, the median generic values for each parameter obtained from the analysis of the goethite data ($\log K_{\text{Me}}$ and z_0/z_1) were used to predict the metal ion (i.e., Cd, Cu, and Pb) adsorption onto HFO (experimental data set presented in Appendix D) without any further adjustment.

3.2.1. Cadmium binding data

3.2.1.1. Sorption onto goethite. The necessity of considering the hydrolyzed species of Cd to describe the experiments performed at high pH values has been highlighted during preliminary calculations not presented here. The median parameters are presented in Table 2. The description of a selection of different experiments with the optimized constants and with the median constant is presented in Figs. 3a and b. The adsorption data are very well described with the median parameters (Figs. 3a and b), except one experiment from Hayes and Leckie (1987) performed at the lowest ionic strength ($I = 0.001 \text{ mol L}^{-1}$) (not shown here).

Furthermore, the predominance of the bidentate corner-sharing complexes predicted with the modeling (Figs. 3c and d) is in agreement with EXAFS observations (Spadini et al., 1994; Randall et al., 1999). Spadini et al. (1994) observed an increase of the edge-sharing complexes for the experiments performed with the lowest Cd concentrations. The modeling results are in good agreement with this observation because they also show an increase of edge-sharing complexes with the decrease of cadmium concentration (Figs. 3c and d).

3.2.1.2. Sorption onto HFO. The simulation of the adsorption of Cd on HFO, without any adjustment is very close to the experimental data (Figs. 3e and f). A simple transposition of the constants obtained for goethite, allowed a very good description of the adsorption isotherm of Cd on HFO. Only a slight difference is observed between the simulation and the data for the experiment performed with the lowest Cd concentration where the modeling underestimates the amount of cadmium sorbed onto HFO (Fig. 3e). The modeling predicts the predominance of the edge-sharing complexes (Figs. 3g and h), whatever the experimental conditions, which is in agreement with spectroscopic results of Spadini et al. (1994).

3.2.2. Lead binding data

3.2.2.1. Sorption onto goethite. As for cadmium, the hydrolyzed form of lead was taken into account to allow a good description of the experimental data. The median parameters are presented in Table 2.

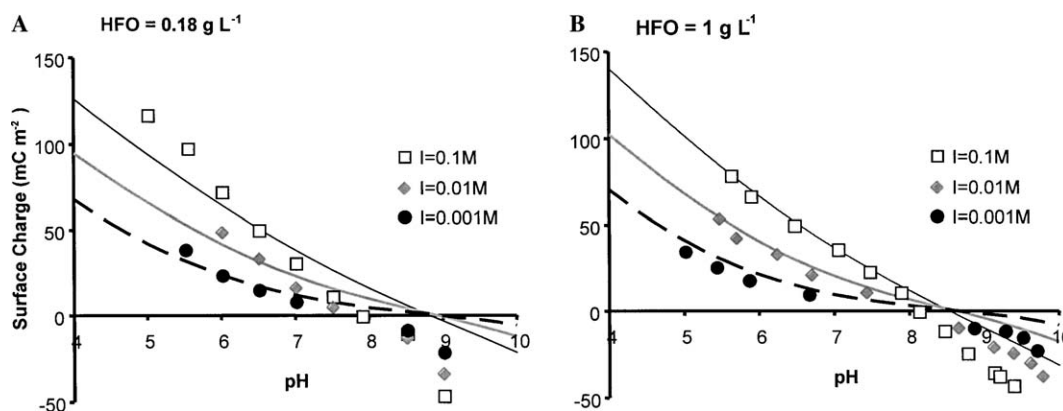


Fig. 2. Charging behavior of HFO at three different salt concentrations and two solid/liquid (S/L) ratios (A data from Davies (1977), S/L = 0.18 g L⁻¹ and B data from Hsi and Langmuir (1985), S/L = 1 g L⁻¹). The lines correspond to model calculation using: $S_{[110]} = 300 \text{ m}^2 \text{ g}^{-1}$, $S_{[021]} = 500 \text{ m}^2 \text{ g}^{-1}$, $C = 1.27 \text{ F m}^{-2}$, and $\log K_i = -1.5$.

The accuracy of the description of the experimental adsorption curves with the median parameters is variable depending of the experimental data (Figs. 4a and b). The calculation using the optimized parameters allow a very good description of the different experimental data sets, except for the data obtained at the lowest Pb concentrations. For these experiments, the modeling underestimates the fraction of lead sorbed onto goethite (Fig. 4a). This gap between data and modeling could be attributed to the lack, in the model, of a species that is relevant for low Pb concentrations. To test this hypothesis, new experimental data at low Pb concentrations are needed. A decreasing contribution of the bidentate corner-sharing complexes with decreasing pH is predicted with the modeling (Figs. 4c and d) and is in agreement with EXAFS observations of Ostergren et al. (2000).

3.2.2.2. Sorption onto HFO. The parameters optimized for the goethite data allow a quite good simulation of the adsorption data on HFO (Figs. 4e and f), with an overestimation of the fraction of lead sorbed for the experiments with the highest Pb concentrations (Fig. 4e). The modeling predicts a large predominance of the edge-sharing complexes for the different experiments described, the corner-sharing complexes being negligible (Figs. 4g and h). These results are in agreement with the spectroscopic observations of Manceau et al. (1992) and Scheinost et al. (2001) who found a major contribution of one Pb–Fe distance (3.30 Å) characteristic of edge-sharing complexes. On the other hand, Trivedi et al. (2003) also observed a long Pb–Fe distance, characteristic of corner-sharing complexes. As observed on goethite by Ostergren et al. (2000), these authors highlighted the evolution of the surface complexes as a function of pH, with a decreasing of the proportion of corner-sharing complexes with decreasing pH. However, this evolution is not described with the modeling because the proportion of corner-sharing complexes is very low (Figs. 4g and h).

3.2.3. Copper binding data

3.2.3.1. Sorption to goethite. Preliminary calculations considering a bidentate edge-sharing complex with two

Fe₂OH groups, did not allow an accurate description of the experimental data. Subsequently, a tridentate complex with two FeOH groups and one Fe₃O group was added to the modeling, allowing an improvement of the experimental data description. This complex was not considered in the first calculations because its formation implies long Cu–Fe distances which were not clearly evidenced with spectroscopic techniques. Nevertheless, spectroscopic results can strongly depend on experimental conditions, as observed for cadmium (Spadini et al., 1994). As for the other metals, the hydrolyzed form of copper was considered. The median parameters are presented in Table 2. The modeling with the median parameter values allows a good description of the experimental data (Figs. 5a and b), with a slight discrepancy for the experiments with the lowest Cu concentrations (Fig. 5a, data from Robertson, 1996). For these conditions, the modeling slightly underestimates the fraction of copper sorbed on goethite. As for lead, this discrepancy could be explained by the lack, in the model, of a surface complex that is important at low copper concentrations. The modeling predicted the predominance of the bidentate edge-sharing and tridentate edge-sharing complexes located on the [110] plane (Figs. 5c and d). We have no spectroscopic information to validate this results.

3.2.3.2. Sorption onto HFO. The prediction of the adsorption curves of copper on HFO with the parameters optimized for goethite is close to the experimental data (Figs. 5e and f). Scheinost et al. (2001) studied the adsorption of copper and lead on HFO with EXAFS. These authors concluded that the surface complexes formed by these two metals were similar. Their observations reinforce our choice of the same complexes for lead and copper for the modeling on the [021] face. This face being the dominant one for HFO, the complexes observed by Scheinost et al. (2001) are probably related to the [021] face. The tridentate edge-sharing complexes present on the [110] and [021] planes, thus dominate the surface speciation (Figs. 5g and h).

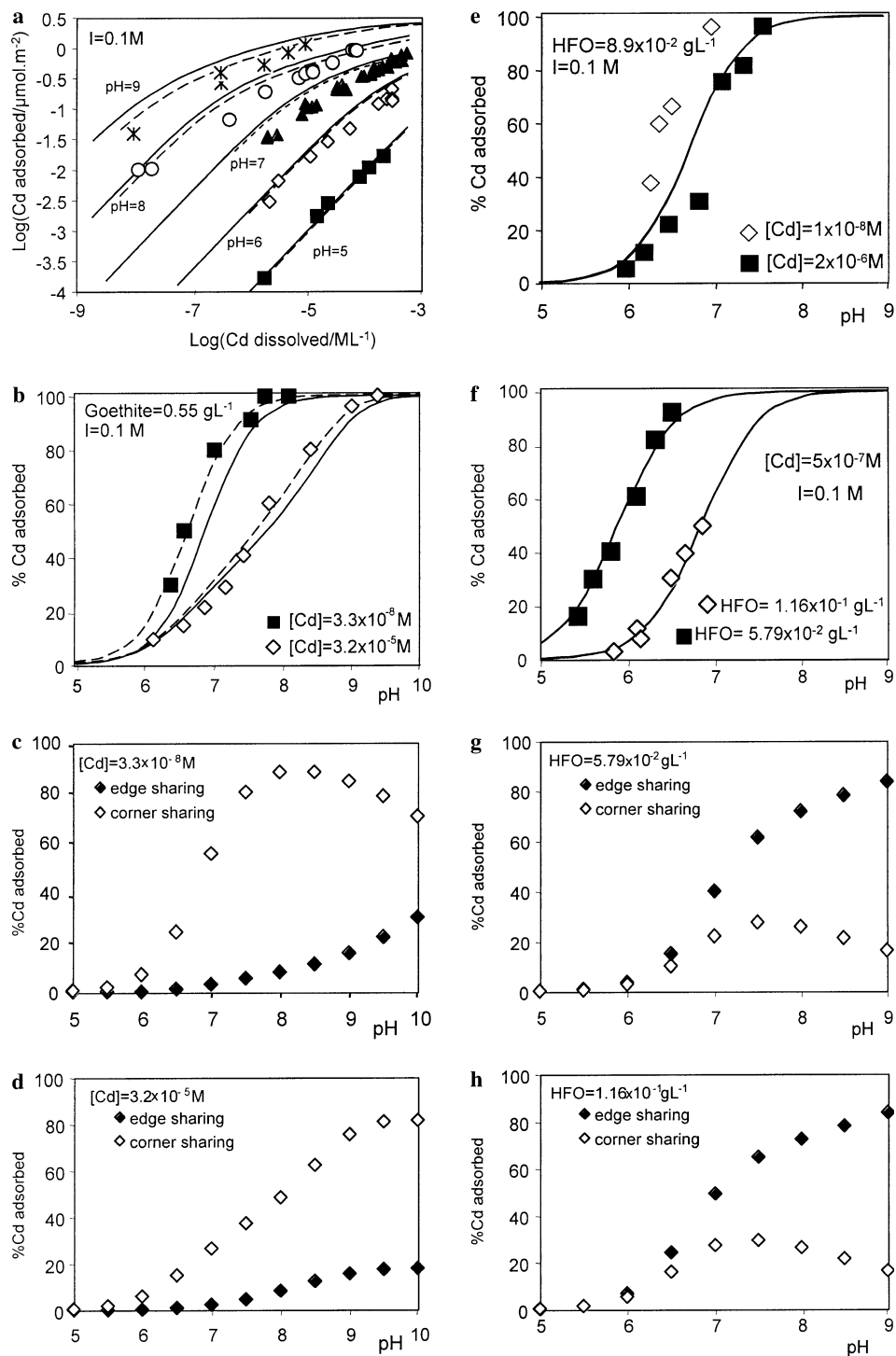


Fig. 3. Cd binding to goethite and HFO as a function of pH and total Cd amount. Experimental data are described using optimized parameters for each individual data set (dotted line) and median parameters (solid lines). (a and b) correspond to data sets G-Cd-6 and G-Cd-1, respectively. (c and d) correspond to calculated “surface” speciation for sorption data given in (b). (e and f) correspond to data sets HFO-Cd-1 and HFO-Cd-3, respectively and (g and h) correspond to calculated “surface” speciation for sorption data given in (f).

3.2.4. Zinc binding data

3.2.4.1. Goethite. The hydrolyzed form of zinc was considered to allow a good description of the experimental data. The median parameters are presented in Table 2. The adsorption data for zinc on goethite are less abundant than for the other metals. However, for the available data set,

the modeling with the median parameter values allows a good description of the experimental data (Figs. 6a and b), except for the data of Balistrieri and Murray (1982) obtained with the highest concentration of zinc (Fig. 6a). In that case, the fraction of zinc sorbed is largely overestimated with the median parameters. The “surface” speciation is

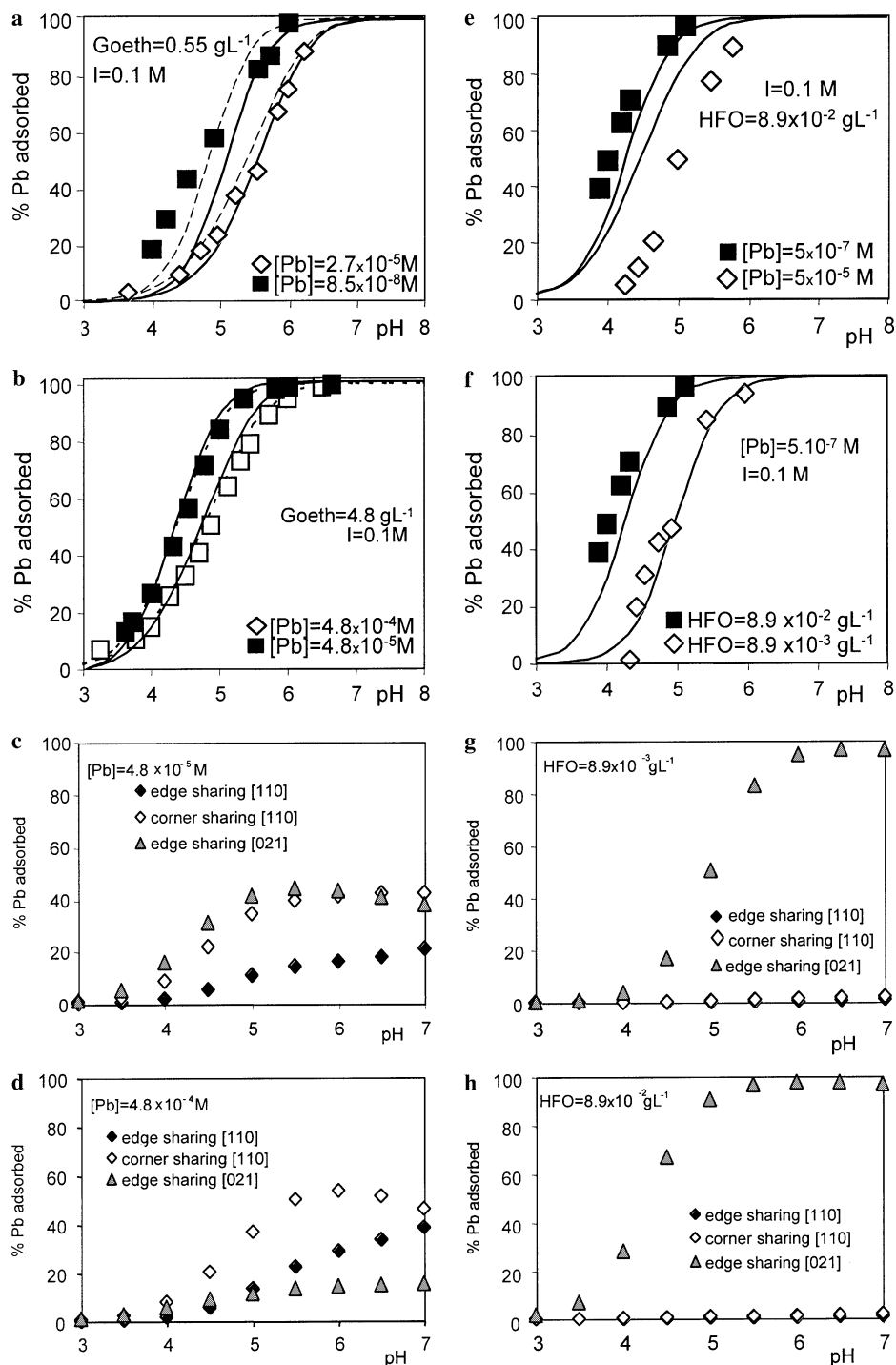


Fig. 4. Pb binding to goethite and HFO as a function of pH and total Pb amount. Experimental data are described using optimized parameters for each individual data set (dotted line) and median parameters (solid lines). (a and b) correspond to data sets G-Pb-3 and G-Pb-8, respectively. (c and d) correspond to calculated “surface” speciation for sorption data given in (b). (e and f) correspond to data sets HFO-Pb-1 and HFO-Pb-2, respectively and (g and h) correspond to calculated “surface” speciation for sorption data given in (f).

dominated in all cases by bidentate edge-sharing complexes (Figs. 6c and d) in agreement with the spectroscopic data of Schlegel et al. (1997) and Juillot et al. (2003).

3.2.4.2. Sorption to HFO. In the case of zinc, a single transposition of the parameters adjusted to describe the interac-

tions with goethite is not possible because the surface complexes are different on goethite (octahedral Zn) and on HFO (tetrahedral Zn). The same approach as for goethite is followed to adjust the parameters used to describe the interactions of zinc with HFO. The hydrolyzed form of zinc was considered to allow a good description of the

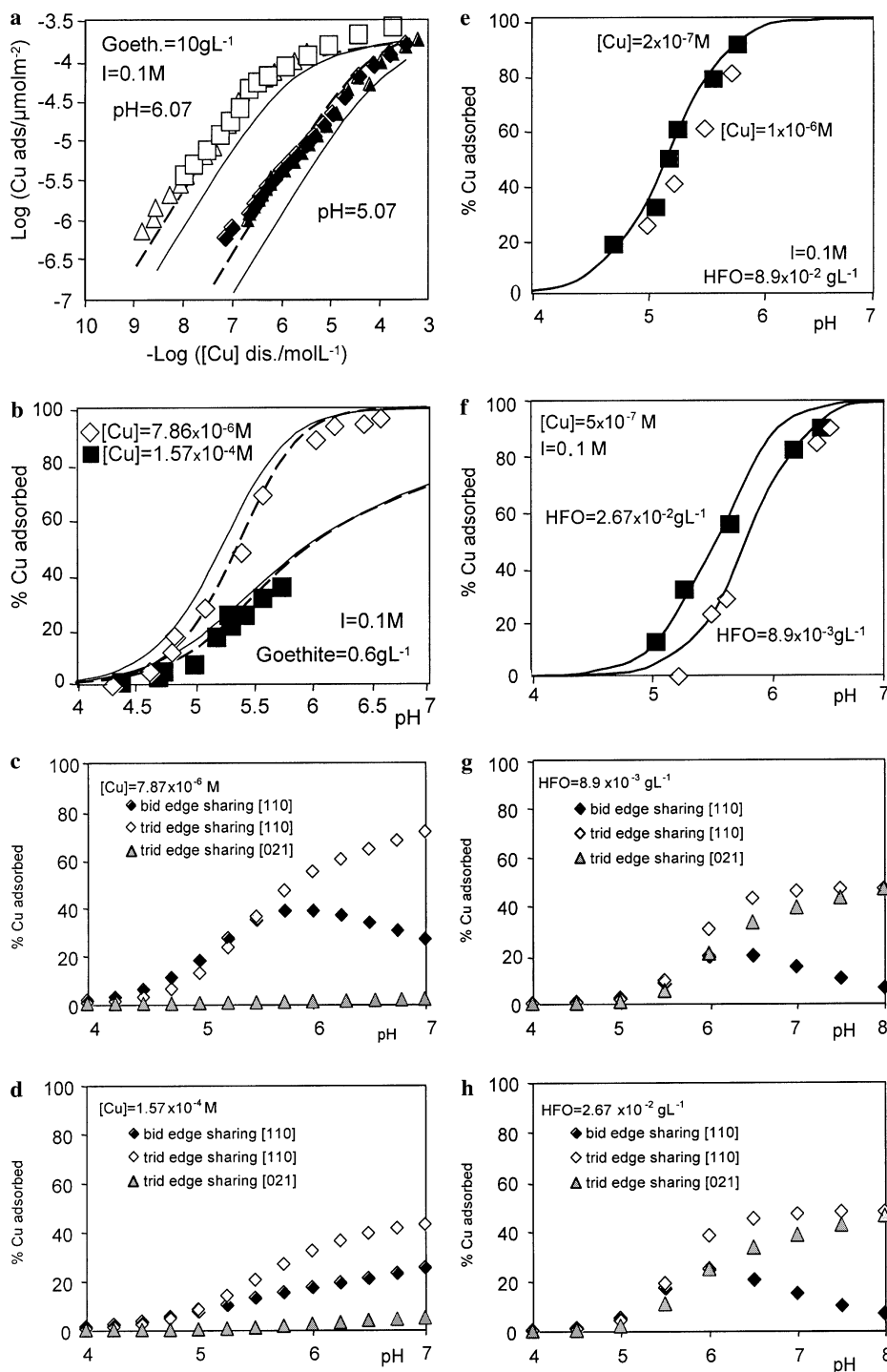


Fig. 5. Cu binding to goethite and HFO as a function of pH and total Cu amount. Experimental data are described using optimized parameters for each individual data set (dotted line) and median parameters (solid lines). (a and b) correspond to data sets G-Cu-7 and G-Cu-4, respectively. (c and d) correspond to calculated "surface" speciation for the sorption data given in (b). (e and f) correspond to data sets HFO-Cu-1 and HFO-Cu-2, respectively. (g and h) correspond to calculated "surface" speciation for the sorption data given in (f).

experimental data. The median parameters and model lines are given in Table 2 and Figs. 7a and b, respectively.

For the [021] face, the bidentate complexes combine a FeO_IH group and a FeO_{II}H group. To write this complex in the model, the two distinct groups, or two FeOH_m groups, as for the other metal, can be used. This compari-

son allowed a check for the absence of modification induced by the use of the 'mean' FeOH_m groups. Calculations have been done with the two options and the difference is smaller or equal to 5%.

The modeling results of Zn adsorption data on HFO with the median parameter values are very close to the

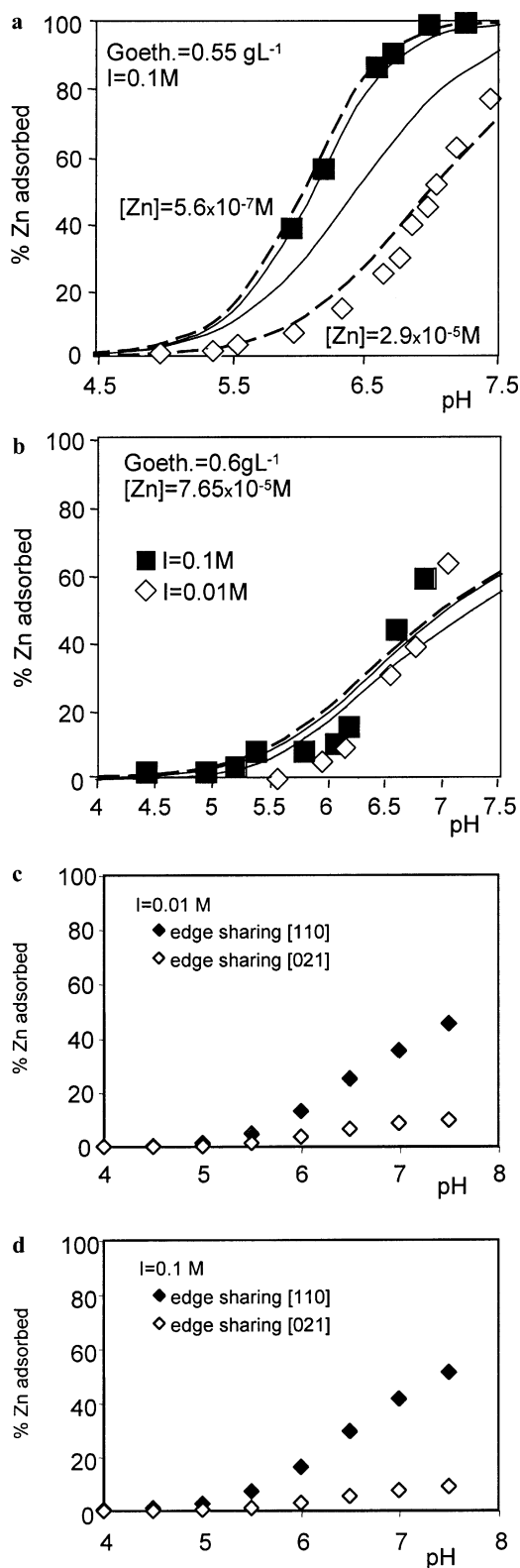


Fig. 6. Zn sorption onto goethite as a function of pH and total Zn amount. Experimental data are described using optimized parameters for each individual data set (dotted line) and median parameters (solid lines). (a and b) correspond to data sets G-Zn-1 and G-Zn-3, respectively. (c and d) correspond to calculated “surface” speciation for sorption data given in (b).

experimental data set (Figs. 7a and b). A slight difference is observed for the data of Kinniburgh and Jackson (1982) obtained with the highest ionic strength (1 mol L^{-1}) (data not shown). The model predicts a change in the “surface” speciation of Zn on HFO for low and high Zn concentration conditions. Corner-sharing complexes on both [110] and [021] planes control the surface speciation at low concentrations (Fig. 7c). At higher Zn concentrations corner-sharing complexes on the [021] plane are predicted to dominate, especially at pH above 7. New EXAFS data obtained for similar surface coverage are needed to confirm this change.

4. Discussion

4.1. Limitations of the proposed approach

The major focus of this study was to try to get a consistent description of TE sorption behavior that works for goethite and HFO with the same set of model parameters. We did our best to use physically realistic species based on spectroscopic data.

In general, a good prediction of almost all the collected experimental data sets corresponding to metal ion binding to HFO was obtained. Moreover, dominant surface species are in agreement with the recently published surface complexes derived from XAS data for Cd, Cu, and Pb (Spadini et al., 1994; Ostergren et al., 2000; Scheinost et al., 2001). However, some data sets are clearly not well described by the model in the case of goethite (data set of Johnson (1990) with $\text{Cd} = 0.2 \text{ mmol L}^{-1}$ or data set of Kooner (1993) with $I = 0.01 \text{ mol L}^{-1}$, results not shown here) or HFO (e.g., Fig. 4e).

For Pb and Cu we may have missed high affinity sites that are relevant for some of the very low metal concentrations used in some experiments because our species selection was based on EXAFS information obtained with relatively high metal concentrations. In some cases then, we may lack knowledge about high affinity sites specific to some metal ions at concentrations that may be more relevant for natural systems. Indeed, Spadini et al. (1994) showed for Cd that the nature of the surface sites vary strongly with Cd concentration. New data obtained at much lower concentration than already existing data with the new generation of synchrotrons are needed to test this hypothesis and to improve the modeling.

For some data sets (i.e., G-Cd-4, G-Pb-5, and G-Cu-1 in Appendix B) differences between experimental data and modeling are not correlated to experimental conditions. We do not believe that they are related to the modeling options but rather to a large heterogeneity in the experimental data sets for very similar experimental conditions. For instance, Johnson (1990) and Spark et al. (1995) found some very different results when studying Cd sorption onto goethite under similar conditions. Such differences could be related to the heterogeneous nature of oxides (Schwert-

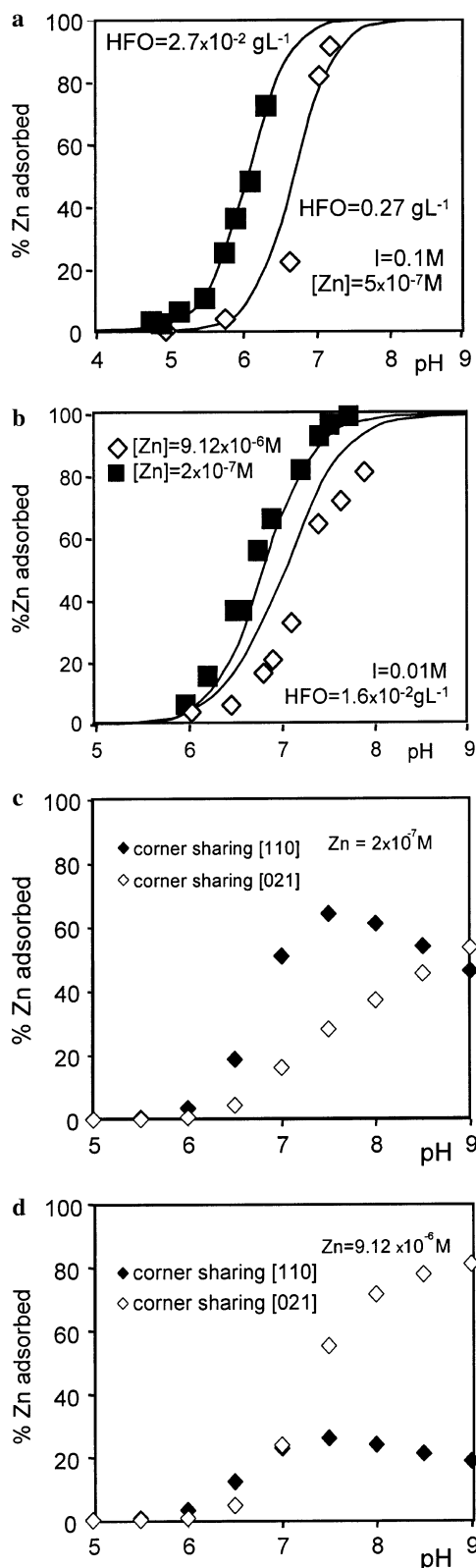


Fig. 7. Zn sorption onto HFO as a function of pH and total Zn amount. Experimental data are described using optimized parameters for each individual data set (dotted line) and median parameters (solid lines). (a and b) correspond to data sets HFO-Zn-1 and HFO-Zn-2, respectively. (c and d) correspond to calculated "surface" speciation for sorption data given in (b). The optimized (dotted) and the median (solid) lines are for those experiments superimposed.

mann and Cornell, 1991). In addition, synthesis protocols for goethite and HFO may vary from one author to another. Differences in protocols generate differences in the respective proportion of the two main crystallographic planes ([110] and [021]) where reactive sites are located (Dzombak and Morel, 1990; for HFO). This heterogeneity will induce discrepancies among experimental data obtained a priori under similar physico-chemical conditions (salt level, pH range, and metal to ligand ratio). Such differences can hardly be accounted for by any modeling approach using a generic set of parameters adjusted with a large database. For this purpose, to obtain a set of generic adjusted parameters with such variations can be an advantage because it can produce more realistic predictions of the complex geochemistry of natural or anthropogenic systems where heterogeneous ligands like organic matter (Tipping, 1998; Kinniburgh et al., 1999) or oxides are always involved. Moreover, Sauvé et al. (2000) showed that iron oxides produced in the laboratory had a different reactivity when compared to "natural" iron oxides.

Other possible variables that could explain the discrepancy between modeling and experimental data are pH, ionic strength, and composition of the solution.

Concerning pH, Ostergren et al. (2000) showed that the nature of the Pb surface sites could vary strongly between pH 4 and 7. It would be interesting to have similar data sets and the corresponding XAS data for Cu and Zn in order to better constrain the surface species used for those elements in future versions of the modeling.

Concerning ionic strength, most transition metal sorption on oxide surfaces occurs by specific surface complex formation with oxygen atoms at the surface (Crescenti and Sverjenski, 1999). For instance, no salt effect is observed during Pb and Cd (Hayes and Leckie, 1987) or Cu and Zn sorption (Kooner, 1992). However, in the case of Cd, some recent EXAFS results (Bargar, personal communication) suggest that the so-called outer-sphere complexes (i.e., Cd located on the same electrostatic plane as K or Na) could also be important. Incorporation of such species in our modeling could improve its quality.

Concerning the composition of the solution, Ostergren et al. (2000) showed that, in the case of Pb, sorption onto goethite was achieved through the formation of carbonate complexes. Considering these types of ternary complexes in future modeling should improve its quality, especially when modeling metal ion behavior in soils where CO_2 may be important. However, at the moment, good metal binding data in the presence of carbonate anions are missing in order to calibrate the model.

4.2. Extrapolation to other metal ions: Co, Ni

Unfortunately, for cobalt and nickel, a limited number of sorption experiments combine macroscopic observations with in situ spectroscopic determination of the surface complexes involved. The latter information is however very important for the CD-MUSIC approach.

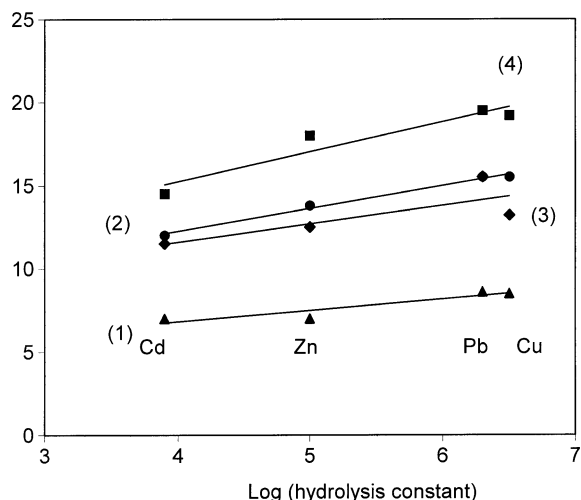


Fig. 8. Linear relationship between hydrolysis constants of Cd, Zn, Pb, and Cu and their specific surface site binding affinity constant within the CD-MUSIC approach. (1) bidentate complexes on the [110] plane, (2) hydrolyzed metal ion forming bidentate complexes on the [110] plane, (3) tridentate complexes on the [021] plane, and (4) hydrolyzed metal ion forming tridentate complexes on the [021] plane. Numbers 1, 2, 3, and 4 correspond to linear regression lines which equation is given in Table 3.

For those metal ions a method is needed to deduce meaningful parameter values from incomplete evidence. One approach is to use the variation in hydrolysis behavior of the different metal ions as an indication of likely relative binding capabilities to iron oxides. Bidentate corner-sharing complexes for Cd and Pb or bidentate edge-sharing complexes for Cu and Zn and a tridentate complex are used for the [110] and [021] crystallographic plane, respectively. In Fig. 8, the binding constant for Cd, Cu, Pb, and Zn are shown for the different surface complexes on goethite (Y axis) as a function of their respective hydrolysis constant (X axis) taken from Morel (1983). Four relationships are obtained, two for each crystallographic plane, and are given in Table 3. Using those relationships and the hydrolysis constant of other metal ions, we can estimate the binding constant for a series of goethite surface sites. Cobalt and nickel were chosen because they have the same valence as the one used to calibrate the modeling approach. Cobalt and nickel are two potentially toxic elements for which sorption experiments to goethite and/or HFO are available in the literature. The binding constant values derived with the empirical relationships for these two elements are reported in Table 3. We use them here to predict the experimental data collected from our literature survey (Appendix B and D).

4.2.1. Cobalt

The results for cobalt are shown in Fig. 9. For this element, we have used bidentate corner-sharing surface complexes, the same as for Cd. This hypothesis is prompted by the equivalent sorption isotherms reported by Spark et al. (1995), for Co and Cd under similar conditions. The

simulations for Co binding to goethite and HFO are in reasonable agreement with the literature data (Figs. 9a and b). This result supports the proposed idea that the same surface complexes can be used, in most cases, to describe divalent metal ion binding to goethite and HFO surfaces, at the same time.

4.2.2. Nickel

Choosing the surface species on the [110] plane involved in nickel binding is more difficult since we do not have extra information to guide our choice, like for cobalt. Two options were tested: bidentate corner-sharing and bidentate edge-sharing. The results of the simulations are shown in Fig. 10. In the case of goethite, for data published by McKenzie (1980) the bidentate corner-sharing complex option seems to give better results although the simulation is not perfect (Fig. 10a). Whatever the option considered, the prediction of the data published by Trivedi et al. (2001) is not satisfying, especially at low pH where the model underestimates the amount of Ni sorbed (Fig. 10b). However, according to Manceau et al. (2000) Ni behaves differently from Cu, Co, and Zn. Its particular behavior could result from a clustering of Ni atoms at the goethite surface. In the case of HFO, the differences in the simulations resulting from the use of either bidentate corner-sharing or edge-sharing complexes are negligible because the [021] crystallographic plane dominates the overall binding. The simulation is in very good agreement with the data published by Leckie et al. (1984) (Fig. 10c). Again, like in the case of goethite, we underestimate the amount of Ni sorbed at low pH for the data set corresponding to experiments by Trivedi et al. (2001) (Fig. 10d).

At the present stage of our work, the predictions that were obtained for Co and Ni for goethite and HFO, as well as the simulations concerning the binding of Cd, Cu, and Pb to HFO, are promising. Until more detailed information on the structure of the two iron oxides are available, the present modeling approach seems a reasonable approximation and can be used to describe complex geochemical systems. To improve our understanding and modeling of multi-component systems involving either crystallized or amorphous iron oxides and various metal ions, we need more data obtained for various experimental conditions. Data obtained at much lower metal ion to iron oxide ratios are particularly needed in order to be able to eventually consider high affinity sites that are not always evidenced in spectroscopic studies because, until now, relatively concentrated systems were needed to obtain good quality spectroscopic data. In the case of Ni and Co, new spectroscopic data are necessary to confirm the choices made a priori for the nature of complexes on the [110] crystallographic plane of goethite and HFO. To be confident in the model predictions obtained with the present approach we believe that it should be tested against competitive adsorption data for various metal ions over a range of pH and ionic strength values.

Table 3

Predicted affinity constants for Co and Ni using the regressions lines 1, 2, 3, and 4 obtained by plotting metal ion surface complexes binding constants as function of metal ion hydrolysis constants (Fig. 8)

	$\log K_{\text{Me-OH}}$	$\log K_{\text{Me-bid}[110]}$	$\log K_{\text{MeOH-bid}[110]}$	$\log K_{\text{Me-tri}[021]}$	$\log K_{\text{MeOH-tri}[021]}$
Cobalt	4.3	7	12.7	11.9	15.8
Nickel	4.1	6.9	12.4	11.7	15.4

For bidentate complexes on the [110] plane: (1) $\log K_{\text{Me-bid}} = 0.68 \times \log K_{\text{hydr}} + 4.08$ ($R^2 = 0.85$) and (2) $\log K_{\text{MeOH-bid}} = 1.37 \times \log K_{\text{hydr}} + 6.78$ ($R^2 = 0.99$) For tridentate complexes on the [021] plane: (3) $\log K_{\text{Me-tri}} = 1.11 \times \log K_{\text{hydr}} + 7.17$ ($R^2 = 0.63$) and (4) $\log K_{\text{MeOH-tri}} = 1.79 \times \log K_{\text{hydr}} + 8.07$ ($R^2 = 0.90$).

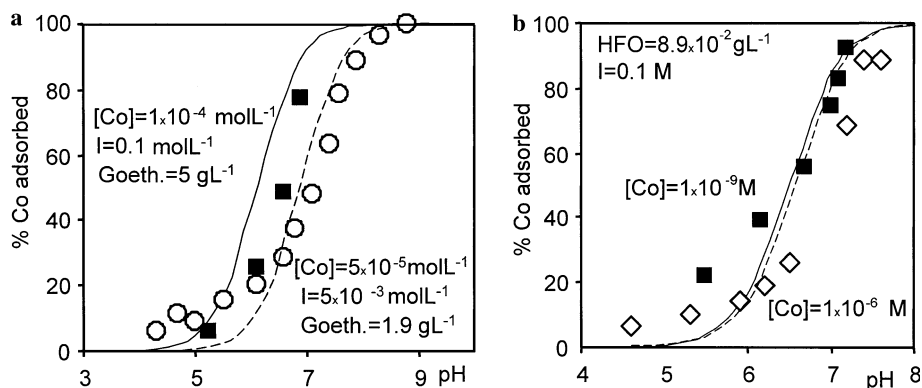


Fig. 9. Cobalt sorption onto goethite (a) (data set: G-Co-1 and G-Co-2) and on HFO (b) (data set: HFO-Co-1): experimental data (dots) and simulation (solid lines for closed symbols and dotted lines for open symbols) using predicted parameters given in Table 3, using bidentate corner-sharing complexes similar to Cd.

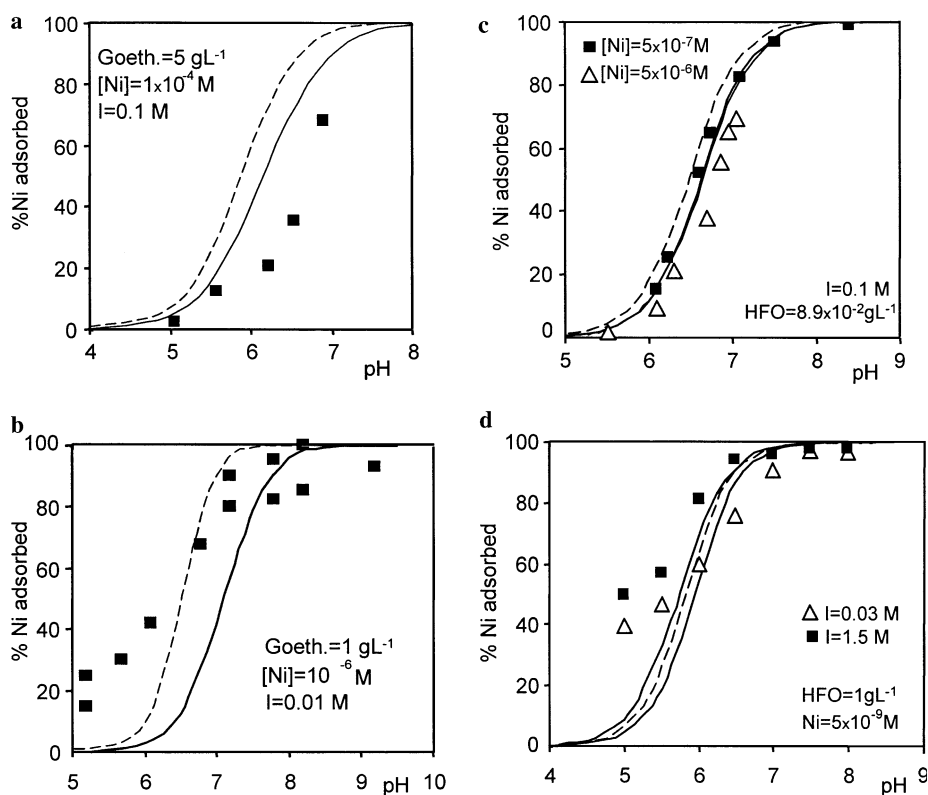


Fig. 10. Nickel sorption onto goethite (a and b) and on HFO (c and d). (a) and (b) corresponding to data sets G-Ni-1 and G-Ni-2, respectively, and (c) and (d) to data sets HFO-Ni-1 and HFO-Ni-2, respectively. Experimental data (dots) and simulation using predicted parameters calculated in Table 3, using bidentate corner-sharing complexes (solid lines) and bidentate edge-sharing complexes (dotted lines).

Acknowledgments

This work was supported by EU Contract No. ENV4-CT97-0554 as well as by the Programme National Sol et Erosion (PNSE) sponsored by the Centre National de la Recherche Scientifique (CNRS), l'Institut National de Sciences de l'Univers (INSU) et l'Institut de Recherche pour le

Développement (IRD). We also acknowledge support of the association Naturalia et Biologia (NEB) to Dr. Marie Ponthieu. Two anonymous reviewers supplied very useful comments. M. Machesky, associated editor, proposed important comments which improved the present manuscript.

Associate editor: Michael L. Machesky

Appendix A. Surface species, site densities, and proton binding constants for goethite are taken from Venema et al. (1998)

	Species	$\log K_{H1}/\log K_{H2}$	Site density (sites nm ⁻²)
[110] Plane	Fe ₁ O _{II}	19.6/7.7	3.03
	Fe ₂ O _{II}	12.3/0.4	3.03
	Fe ₃ O _{II}	-0.2	3.03
	Fe ₃ O _I	11.7	6.06
[021] Plane	Fe ₁ O _{II}	20/8.1	3.75
	Fe ₁ O _I	23.8/11.9	3.75
	Fe ₂ O _{II}	7.9/-4	3.75
	Fe ₂ O _I	15.6/7.7	3.75

Appendix B. Summary details of selected sets of experimental data for metal ion binding by goethite

Code	pH	Ionic strength (mol L ⁻¹)	Metal concentration (mol L ⁻¹)	Goethite (g L ⁻¹)	SSA (m ² g ⁻¹)	Reference
G-Co-1	4-7	0.1 NaNO ₃	1 × 10 ⁻⁴	5	75	Mckenzie (1980)
G-Co-2	4-9	0.005 KNO ₃	5 × 10 ⁻⁵	1.9	49.6	Angove et al. (1999)
G-Ni-1	4-7	0.1 NaNO ₃	1 × 10 ⁻⁴	5	75	Mckenzie (1980)
G-Ni-2	5-10	0.01 NaNO ₃	1 × 10 ⁻⁶	1	27	Trivedi et al. (2001)
G-Zn-1	4-7	0.1 NaNO ₃	5.6 × 10 ⁻⁷ /2.9 × 10 ⁻⁶ / 2.9 × 10 ⁻⁵	0.55	51.8	Balistreri and Murray (1982)
G-Zn-2	4-7	0.1 NaNO ₃	1 × 10 ⁻⁵	2	78	Padmanabham (1983)
G-Zn-3	4-7.5	0.1/0.01 NaNO ₃	7.65 × 10 ⁻⁵	0.6	50	Kooner (1993)
G-Zn-4	4-11	0.001 KNO ₃	1 × 10 ⁻⁴	0.73	62	Spark et al. (1995)
G-Cu-1	4-7	0.1 NaNO ₃	1 × 10 ⁻⁴	5	75	Mckenzie (1980)
G-Cu-2	4-6	0.075 KNO ₃	6.5 × 10 ⁻⁵	0.5	89	Barrow et al. (1981)
G-Cu-3	4-7	0.1 NaNO ₃	3.2 × 10 ⁻⁷ /1.8 × 10 ⁻⁶ / 3.1 × 10 ⁻⁵	0.55	51.8	Balistreri and Murray (1982)
G-Cu-4	4-7	0.1/0.01 NaNO ₃	7.87 × 10 ⁻⁶ /1.57 × 10 ⁻⁵ / 7.87 × 10 ⁻⁵ /1.57 × 10 ⁻⁴	0.6/1.2/ 2.9/5.5	50	Kooner (1992)
G-Cu-5	4-7.5	0.1/0.01 NaNO ₃	7.87 × 10 ⁻⁶ /1.57 × 10 ⁻⁵ / 7.87 × 10 ⁻⁵ /1.57 × 10 ⁻⁴	0.6	50	Kooner (1993)
G-Cu-6	4-11	0.001 KNO ₃	1 × 10 ⁻⁴	0.73	62	Spark et al. (1995)
G-Cu-7	5-6	0.01/0.1 NaNO ₃	From 1 × 10 ⁻³ to 1 × 10 ⁻¹⁰	10	49	Robertson (1996)
G-Cd-1	4-7	0.1 NaNO ₃	3.3 × 10 ⁻⁸ /2.5 × 10 ⁻⁷ / 3 × 10 ⁻⁶ /3. 2 × 10 ⁻⁵	0.55	51.8	Balistreri and Murray (1982)
G-Cd-2	3-7	0.01/0.1/0.3/1 NaNO ₃	1 × 10 ⁻⁴	30	52	Hayes and Leckie (1987)
G-Cd-3	3-8	0.001 KNO ₃	1 × 10 ⁻⁴ /1 × 10 ⁻⁵ /1 × 10 ⁻⁶	2.5	34	Djafer et al. (1989)
G-Cd-4	4-10	0.01 KNO ₃	2 × 10 ⁻⁴ /1 × 10 ⁻⁴ /1 × 10 ⁻⁵ / 3 × 10 ⁻⁶ /1 × 10 ⁻⁶	0.72	76	Johnson (1990)
G-Cd-5	4-11	0.001 KNO ₃	1 × 10 ⁻⁴	0.73	62	Spark et al. (1995)
G-Cd-6	5/6/7/8/9	0.01/0.1/0.5 NaNO ₃	From 1 × 10 ⁻² to 1 × 10 ⁻¹⁰	—	98	Venema et al. (1996b)

Appendix B (continued)

Code	pH	Ionic strength (mol L ⁻¹)	Metal concentration (mol L ⁻¹)	Goethite (g L ⁻¹)	SSA (m ² g ⁻¹)	Reference
G-Pb-1	4-7	0.1 NaNO ₃	1 × 10 ⁻⁴	5	75	Mckenzie (1980)
G-Pb-2	4-6	0.075 KNO ₃	6.5 × 10 ⁻⁵	0.5	89	Barrow et al. (1981)
G-Pb-3	4-7	0.1 NaNO ₃	8.5 × 10 ⁻⁸ /7.6 × 10 ⁻⁷ / 3.4 × 10 ⁻⁶ /2.7 × 10 ⁻⁵	0.55	51.8	Balistreri and Murray (1982)
G-Pb-4	4-7	0.1 NaNO ₃	1 × 10 ⁻⁵	2	78	Padmanabham (1983)
G-Pb-5	3-7	0.01/0.1/0.3/1 NaNO ₃	2 × 10 ⁻³	30	52	Hayes and Leckie (1987)
G-Pb-6	3-8	0.001 KNO ₃	1 × 10 ⁻⁴ /1 × 10 ⁻⁵ /1 × 10 ⁻⁶	2.5	34	Djafer et al. (1989)
G-Pb-7	3-8	0.1 NaNO ₃	4.8 × 10 ⁻⁴	13.9	45	Bargar et al. (1998)
G-Pb-8	3-7	0.1 NaNO ₃	4.8 × 10 ⁻⁴ /4.8 × 10 ⁻⁵	4.8	94	Villalobos et al. (2001)

Appendix C. Optimized proportions of the crystallographic plane [110] compared to the total goethite surface area (Appendix B)

References	% S _[110]
Angove et al. (1999)	90
Balistreri and Murray (1982)	95
Bargar et al. (1998)	95
Barrow et al. (1981)	90
Djafer et al. (1989)	90
Hayes and Leckie (1987)	90
Johnson (1990)	90
Kooner (1992)	95
Kooner (1993)	95
Mckenzie (1980)	90
Padmanabham (1983)	97
Robertson (1996)	
Spark et al. (1995)	90
Trivedi et al. (2001)	
Venema et al. (1996b)	90
Villalobos et al. (2001)	95

Appendix D. Summary details of selected sets of experimental data for metal ion binding by hydrous ferric oxides (HFO)

Code	pH	Ionic strength (mol L ⁻¹)	Metal concentration (mol L ⁻¹)	HFO (g L ⁻¹)	References
HFO-Co-1	4-9	0.1 NaNO ₃	1 × 10 ⁻⁶ /1 × 10 ⁻⁹	8.9 × 10 ⁻²	Benjamin and Bloom (1981)
HFO-Ni-1	4-10	0.1 NaNO ₃	5 × 10 ⁻⁶ /5 × 10 ⁻⁷	8.9 × 10 ⁻²	Leckie et al. (1984)
HFO-Ni-2	4-8	1.5/0.03 NaNO ₃	5 × 10 ⁻⁹	1	Trivedi et al. (2001)
HFO-Zn-1	4-8	0.1 NaNO ₃	2 × 10 ⁻⁶ /5 × 10 ⁻⁷ /1 × 10 ⁻⁷	2.67 × 10 ⁻² / 8.9 × 10 ⁻² / 2.67 × 10 ⁻¹	Benjamin (1978) Leckie et al. (1980)
HFO-Zn-2	4-8	0.01 NaNO ₃	9.12 × 10 ⁻⁶ /3.02 × 10 ⁻⁶ / 7.59 × 10 ⁻⁷ /3.8 × 10 ⁻⁷ /2 × 10 ⁻⁷	1.59 × 10 ⁻²	Dempsey and Singer (1980)
HFO-Zn-3	3-8	1 NaNO ₃	1 × 10 ⁻⁴ /1 × 10 ⁻³ /1 × 10 ⁻²	8.3	Kinniburgh and Jackson (1982)
HFO-Cu-1	4-7	0.1 NaNO ₃	1 × 10 ⁻⁷ /2 × 10 ⁻⁷ /5 × 10 ⁻⁷ / 1 × 10 ⁻⁶	8.9 × 10 ⁻²	Benjamin (1978) Leckie et al. (1980) Benjamin and Leckie (1982)

(continued on next page)

Appendix D (continued)

Code	pH	Ionic strength (mol L ⁻¹)	Metal concentration (mol L ⁻¹)	HFO (g L ⁻¹)	References
HFO-Cu-2	4–7	0.1 NaNO ₃	5 × 10 ⁻⁷	8.9 × 10 ⁻³ / 2.67 × 10 ⁻² / 8.9 × 10 ⁻²	Benjamin (1978) Leckie et al. (1980) Benjamin and Leckie (1982)
HFO-Cd-1	5–9	0.1 NaNO ₃	1 × 10 ⁻⁸ /1 × 10 ⁻⁷ /5 × 10 ⁻⁷ / 2 × 10 ⁻⁶	8.9 × 10 ⁻²	Benjamin (1978) Leckie et al. (1980) Benjamin and Leckie (1981)
HFO-Cd-2	5–9	0.1 NaNO ₃	2 × 10 ⁻⁸ /5 × 10 ⁻⁸ /2 × 10 ⁻⁷	8.9 × 10 ⁻¹	Benjamin (1978) Leckie et al. (1980) Benjamin and Leckie (1981)
HFO-Cd-3	5–9	0.1 NaNO ₃	5 × 10 ⁻⁷	1.16 × 10 ⁻² / 5.79 × 10 ⁻² / 1.16 × 10 ⁻¹ / 3.47 × 10 ⁻¹ / 1.16	Benjamin (1978) Leckie et al. (1980) Benjamin and Leckie (1981)
HFO-Cd-4	4–9	0.1 NaNO ₃	5 × 10 ⁻⁷	8.9 × 10 ⁻² / 8.9 × 10 ⁻³	Davies and Leckie (1979)
HFO-Cd-5	4–9	0.7 NaNO ₃	5 × 10 ⁻⁷	8.9 × 10 ⁻²	Benjamin and Leckie (1982)
HFO-Cd-6	5–9	0.1 NaNO ₃	1 × 10 ⁻⁶	8.9 × 10 ⁻²	Honeyman (1984)
HFO-Pb-1	2–7	0.1 NaNO ₃	5 × 10 ⁻⁷ /5 × 10 ⁻⁶ /5 × 10 ⁻⁵	8.9 × 10 ⁻²	Benjamin (1978) Leckie et al. (1980)
HFO-Pb-2	2–7	0.1 NaNO ₃	5 × 10 ⁻⁷	8.9 × 10 ⁻² / 2.67 × 10 ⁻² / 8.9 × 10 ⁻³	Benjamin (1978) Leckie et al. (1980)

References

- Alcacio, T.E., Hesterberg, D., Chou, J.W., Martin, J.D., Beauchemin, S., Sayers, D.E., 2001. Molecular scale characteristics of Cu(II) bonding in goethite-humate complexes. *Geochim. Cosmochim. Acta* **65**, 1355–1366.
- Angove, M.J., Wells, J.D., Johnson, B.B., 1999. The influence of temperature on the adsorption of Cadmium(II) and Cobalt(II) on goethite. *J. Colloid Interface Sci.* **211**, 281–290.
- Balistreri, L.S., Murray, J.W., 1982. The adsorption of Cu, Pb, Zn and Cd on goethite from major ion seawater. *Geochim. Cosmochim. Acta* **46**, 1253–1265.
- Bargar, J.R., Brown, G.E.J., Parks, G.A., 1997. Surface complexation of Pb(II) at oxide–water interfaces: II. XAFS and bond-valence determination of mononuclear Pb(II) sorption products and surface functional groups on iron oxides. *Geochim. Cosmochim. Acta* **61**, 2639–2652.
- Bargar, J.R., Brown Jr., G.E., Parks, G.A., 1998. Surface complexation of Pb(II) at oxide–water interfaces: III. XAFS determination of Pb(II) and Pb(II)-chloro adsorption complexes on goethite and alumina. *Geochim. Cosmochim. Acta* **62**, 193–207.
- Barrow, N.J., Bowden, J.W., Posner, A.M., Quirk, J.P., 1981. Describing the adsorption of copper, zinc and lead on a variable charge mineral surface. *Aust. J. Soil Res.* **19**, 309–321.
- Benjamin M.M. (1978) Effects of competing metals and complexing ligands on trace metal adsorption at the oxide/solution interface. Ph.D. thesis, Stanford University, Stanford, California.
- Benjamin, M.M., Bloom, N.S., 1981. Effects of strong binding of anionic adsorbates on adsorption of trace metals on amorphous iron oxyhydroxides. In: Tewari, P.H. (Ed.), *Adsorption from Aqueous Solution*. Plenum Press, New York.
- Benjamin, M.M., Leckie, J.O., 1981. Multiple-site adsorption of Cd, Cu, Zn, and Pb on amorphous iron oxyhydroxides. *J. Colloid Interface Sci.* **79**, 209–221.
- Benjamin, M.M., Leckie, J.O., 1982. Effects of complexation by Cl, SO₄, and S₂O₃ on adsorption behavior of Cd on oxide surfaces. *Environ. Sci. Technol.* **16**, 162–170.
- Bochatay, L., Persson, P., Lövgren, L., Brown, G.E.J., 1997. XAFS study of Cu(II) at the water–goethite (α-FeOOH) interface. *J. de Phys. IV* **7**, 819–820, Colloque C2.
- Boily, J.-F., Persson, P., Sjöberg, S., 2000. Benzenecarboxylate surface complexation at the goethite ([α]-FeOOH)/water interface: II. Linking IR spectroscopic observations to mechanistic surface complexation models for phthalate, trimellitate, and pyromellitate. *Geochim. Cosmochim. Acta* **64** (20), 3453–3470.
- Brown, G.E.J., Foster, A.L., Ostergren, J.D., 1999. Mineral surfaces and bioavailability of heavy metals: a molecular-scale perspective. *Proc. Natl. Acad. Sci. USA* **96**, 3388–3395.
- Brown, I.D., Altermatt, K.K., 1985. Bond valence parameters obtained from a systematic analysis of the inorganic crystal structure database. *Acta Crystallogr. B* **41**, 244–247.
- Buffle, J., 1990. *Complexation Reactions in Aquatic Systems. An Analytical Approach*. Ellis Horwood Limited.
- Crescenti, L.J., Sverjenski, D.A., 1999. The role of electrolyte anions (ClO₄⁻, NO₃⁻, and Cl⁻) in divalent metal (M²⁺) adsorption on oxide and hydroxide surfaces in salt solutions. *Am. J. Sci.* **299**, 828–899.
- Davies, J.A., 1977. *Adsorption of Trace Metals and Complexing Ligands at Oxide/Water Interface*. Stanford University.
- Davies, J.A., Leckie, J.O., 1979. Speciation of adsorbed ions at the oxide/water interface, Symposium Series 93. In: Jenne, E.A. (Ed.), *Chemical Modeling of Aqueous Systems*. American Chemical Society, p. 299.

- Dempsey, B.A., Singer, P.C., 1980. The effects of calcium on the adsorption of zinc by MnOx(s) and Fe(OH)₃ (am). In: Baker, R.A. (Ed.), *Contaminants and Sediments*, 2. Ann Arbor Science, pp. 333–352.
- Djafer, M., Lamy, I., Terce, M., 1989. Interaction of metallic cations with the hydrous goethite (γ -FeOOH) surface. *Prog. Colloid Polym. Sci.* **79**, 150–154.
- Dzombak, D.A., Morel, F.M.M., 1990. *Surface Complexation Modeling: Hydrous Ferric Oxides*. John Wiley & Sons.
- Gaboriaud, F., Ehrhardt, J.-J., 2003. Effects of different crystal faces on the surface charge of colloidal goethite ([α]-FeOOH) particles: an experimental and modeling study. *Geochim. Cosmochim. Acta* **67** (5), 967–983.
- Hayes, K.F., Leckie, J.O., 1987. Modeling ionic strength effects on cation adsorption at hydrous oxide/solution interfaces. *J. Colloid Interface Sci.* **115**, 564–572.
- Hiemstra, T., De Wit, J.C.M., Van Riemsdijk, W.H., 1989a. Multisite proton adsorption modeling at the solid/solution interface of (hydr)oxides: a new approach, II. Application to various important (hydr)oxides. *J. Colloid Interface Sci.* **133**, 105–117.
- Hiemstra, T., Van Riemsdijk, W.H., Bolt, G.H., 1989b. Multisite proton adsorption modeling at the solid/solution interface of (hydr)oxides: a new approach, I. Model description and evaluation of intrinsic reaction constants. *J. Colloid Interface Sci.* **133**, 91–104.
- Hiemstra, T., Van Riemsdijk, W.H., 1996. A surface structural approach to ion adsorption: the charge distribution (CD) model. *J. Colloid Interface Sci.* **179**, 488–508.
- Hiemstra, T., Venema, P., Van Riemsdijk, W.H., 1996. Intrinsic proton affinity of reactive surface groups of metal (hydr)oxides: the bond valence principle. *J. Colloid Interface Sci.* **184**, 680–692.
- Honeyman B.D., 1984. Cation and anion adsorption at the oxide/solution interface in systems containing binary mixtures of adsorbents: an investigation of the concept of adsorptive additivity. Ph.D. thesis, Stanford University, California.
- Hsi, C.D., Langmuir, D., 1985. Adsorption of uranyl onto ferric oxyhydroxides: application of the surface complexation site-binding model. *Geochim. Cosmochim. Acta* **49**, 1931–1941.
- Huang, C.P., Stumm, W., 1973. Specific adsorption of cations on hydrous γ -Al₂O₃. *J. Colloid Interface Sci.* **43**, 409–420.
- Johnson, B.B., 1990. Effect of pH, temperature, and concentration on the adsorption of cadmium on goethite. *Environ. Sci. Technol.* **24**, 112–118.
- Juillot, F., Morin, G., Ildefonse, P., Trainor, T.P., Benedetti, M.F., Galois, L., Calas, G., Brown, G.E.J., 2003. Occurrence of Zn/Al hydroxalite in smelter-impacted soils from Northern France: evidence from EXAFS spectroscopy and chemical extractions. *Am. Mineral.* **88**, 509–526.
- Keizer, M.G., Van Riemsdijk, W.H., 1999. *ECOSAT: Equilibrium Calculation of Speciation and Transport, User Manual, Version 4.7*. Wageningen Agricultural University, The Netherlands.
- Kinniburgh, D.G., Jackson, M.L., 1982. Concentration and pH dependence of calcium and zinc adsorption by iron hydrous oxide gel. *Soil Sci. Soc. Am. J.* **46**, 56–61.
- Kinniburgh, D.G., Van Riemsdijk, W.H., Koopal, L.K., Borkovec, M., Benedetti, M.F., Avena, M.J., 1999. Ion binding to natural organic matter: competition, heterogeneity, stoichiometry and thermodynamic consistency. *Colloids Surf A—Physicochemical and Engineering Aspects* **151**, 147–166.
- Kooner, Z.S., 1992. Adsorption of copper onto goethite in aqueous systems. *Environ. Geol.* **20**, 205–212.
- Kooner, Z.S., 1993. Comparative study of adsorption behavior of copper, lead, and zinc onto goethite in aqueous systems. *Environ. Geol.* **21**, 242–250.
- Leckie, J.O., Benjamin, M.M., Hayes, K.F., Kaufman, G., Altmann, S., 1980. Adsorption/coprecipitation of trace elements from water with iron oxyhydroxides. EPA RP-910-1, Electric Power Research Institute, Palo Alto, California.
- Leckie, J.O., Appleton, A.R., Ball, N.B., Hayes, K.F., Honeyman, B.D., 1984. Adsorptive removal of trace elements from fly-ash pond effluents onto iron oxyhydroxides. Electric Power Research Institute.
- Manceau, A., Combes, J.M., 1988. Structure of Mn and Fe oxides and oxyhydroxides: a topological approach by EXAFS. *Phys. Chem. Miner.* **15**, 283–295.
- Manceau, A., Charlet, L., Boisset, M.C., Didier, B., Spadini, L., 1992. Sorption and speciation of heavy metals on hydrous Fe and Mn oxides. From microscopic to macroscopic. *Appl. Clay Sci.* **7**, 201–223.
- Manceau, A., Charlet, L., 1994. The mechanism of selenate adsorption on goethite and hydrous ferric oxide. *J. Colloid Interface Sci.* **168**, 87–93.
- Manceau, A., Schlegel, M.L., Musso, M., Sole, V.A., Gauthier, C., Petit, P.E., Trolard, F., 2000. Crystal chemistry of trace elements in natural and synthetic goethite. *Geochim. Cosmochim. Acta* **64**, 3643–3661.
- Mckenzie, R.M., 1980. The adsorption of lead and other heavy metals on oxides of manganese and iron. *Aust. J. Res.* **18**, 61–73.
- Milne, C., Kinniburgh, D.G., Van Riemsdijk, W.H., Tipping, E., 2003. Generic NICA-Donnan model parameters for metal-ion binding by humic substances. *Environ. Sci. Technol.* **37**, 958–971.
- Morel, F.M.M., 1983. *Principles of Aquatic Chemistry*. John Wiley & Sons.
- Ostergren, J.D., Trainor, T.P., Bargar, J.R., Brown, G.E.J., Parks, G.A., 2000. Inorganic ligand effects on Pb(II) sorption to goethite (a-FeOOH): I. Carbonate. *J. Colloid Interface Sci.* **225**, 466–482.
- Padmanabham, M., 1983. Comparative study of the adsorption-desorption behavior of copper(II), zinc(II), cobalt(II) and lead(II) at the goethite solution interface. *Aust. J. Soil Res.* **21**, 515–525.
- Parkman, R.H., Charnock, J.M., Bryan, N.D., Livens, F.R., Vaughan, D.J., 1999. Reactions of copper and cadmium ions in aqueous solution with goethite, lepidocrocite, mackinawite, and pyrite. *Am. Mineral.* **84**, 407–419.
- Peacock, C.L., Sherman, D.M., 2004. Copper(II) sorption onto goethite, hematite and lepidocrocite: a surface complexation model based on ab initio molecular geometries and EXAFS spectroscopy. *Geochim. Cosmochim. Acta* **68** (12), 2623–2637.
- Randall, S.R., Sherman, D.M., Ragnarsdottir, K.V., Collins, C.R., 1999. The mechanism of cadmium surface complexation on iron oxyhydroxides minerals. *Geochim. Cosmochim. Acta* **63**, 2971–2987.
- Rietra, R.P.J.J., Hiemstra, T., Van Riemsdijk, W.H., 2001. Comparison of selenate and sulfate adsorption on goethite. *J. Colloid Interface Sci.* **240** (2), 384–390.
- Robertson, A.P., 1996. Goethite/humic acid interactions and their effects on Cu(II) binding. Ph.D., Stanford University.
- Sauvé, S., Martinez, C.E., McBride, M., Hendershot, W., 2000. Adsorption of free lead (Pb²⁺) by pedogenic oxides, ferrihydrite, and leaf compost. *Soil Sci. Soc. Am. J.* **64**, 595–599.
- Scheinost, A.C., Abend, S., Pandya, K.I., Sparks, D.L., 2001. Kinetic controls on Cu and Pb sorption by ferrihydrite. *Environ. Sci. Technol.* **35**, 1090–1096.
- Schindler, P.W., Kamber, H.R., 1968. Die Acidität von silanol-gruppen. *Helv. Chim. Acta* **51**, 1781–1786.
- Schlegel, M.L., Manceau, A., Charlet, L., 1997. EXAFS study of Zn and Zn EDTA sorption at the goethite (a-FeOOH)/water interface. *J. de Phys. IV* **2**, 823–824.
- Schwertmann, U., Cornell, R.M., 1991. *Iron Oxides in the Laboratory*. VCH, Weinheim.
- Smith, D.S., Ferris, F.G., 2001. Proton binding by hydrous ferric oxide and aluminium oxide surfaces interpreted using fully optimized continuous pK a spectra. *Environ. Sci. Technol.* **35**, 4637–4642.
- Spadini, L., Manceau, A., Schindler, P.W., Charlet, L., 1994. Structure and stability of Cd²⁺ surface complexes on ferric oxides. *J. Colloid Interface Sci.* **168**, 73–86.
- Spark, K.M., Johnson, B.B., Wells, J.D., 1995. Characterizing heavy-metal adsorption on oxides and oxyhydroxides. *Eur. J. Soil Sci.* **46**, 621–631.
- Stumm, W., Huang, C.P., Jenkins, S.R., 1970. Specific chemical interaction affecting the stability of dispersed systems. *Croat. Chem. Acta* **42**, 223–244.
- Stumm, W., Morgan, J.J., 1981. *Aquatic Chemistry. An Introduction Emphasizing Chemical Equilibria in Natural Waters*. John Wiley & Sons.

- Sverjenski, D.A., Sahai, N., 1996. Theoretical prediction of single-site surface-protonation equilibrium constants for oxides and silicates in water. *Geochim. Cosmochim. Acta* **60**, 3773–3797.
- Tipping, E., 1998. Humic ion-binding model VI : an improved description of the interactions of protons and metal ions with humic substances. *Aq. Geochem.* **4**, 3–48.
- Trivedi, P., Axe, L., Dyer, J.A., 2001. Adsorption of metal ions onto goethite: single-adsorbate and competitive systems. *Colloids Surface A* **191**, 107–121.
- Trivedi, P., Dyer, J.A., Sparks, D.L., 2003. Lead sorption onto ferrihydrite. I. A macroscopic and spectroscopic assessment. *Environ. Sci. Technol.* **37**, 908–914.
- Van Riemsdijk, W.H., Bolt, G.H., Koopal, L.K., Blaakmeer, J., 1986. Electrolyte adsorption on heterogeneous surfaces: adsorption models. *J. Colloid Interface Sci.* **109** (1), 219–228.
- Venema, P., Hiemstra, T., Van Riemsdijk, W.H., 1996a. Comparison of different site binding models for cation sorption; Description of pH dependency and cation-proton exchange. *J. Colloid Interface Sci.* **181**, 45–59.
- Venema, P., Hiemstra, T., Van Riemsdijk, W.H., 1996b. Multisite adsorption of cadmium on goethite. *J. Colloid Interface Sci.* **183**, 515–527.
- Venema, P., Hiemstra, T., Weidler, P.G., Van Riemsdijk, W.H., 1998. Intrinsic proton affinity of reactive surface groups of metal (hydr)oxides: application to iron (hydr)oxides. *J. Colloid Interface Sci.* **198**, 282–295.
- Villalobos, M., Trotz, M.A., Leckie, J.O., 2001. Surface complexation modeling of carbonate effects on the adsorption of Cr(VI), Pb(II), and U(VI) on goethite. *Environ. Sci. Technol.* **35**, 3849–3856.
- Waychunas, G.A., Fuller, C.C., Davis, J.A., 2002. Surface complexation and precipitate geometry for aqueous Zn(II) sorption on ferrihydrite I: X-ray absorption extended fine structure spectroscopy analysis. *Geochim. Cosmochim. Acta* **66**, 1119–1137.
- Weesner, F.J., Bleam, W.F., 1998. Binding characteristics of Pb²⁺ on anion-modified and pristine hydrous oxide surfaces studied by electrophoretic mobility and X-ray absorption spectroscopy. *J. Colloid Interface Sci.* **205**, 380–389.
- Weng, L., Temminghoff, E.J.M., Van Riemsdijk, W.H., 2001. Contribution of individual sorbents to the control of heavy metal activity in sandy soil. *Environ. Sci. Technol.* **35**, 4436–4443.
- Westall, J.C., 1986. Reactions at the oxide-solution interface: chemical and electrostatic models. In: J.A. Davis, K.F. Hayes (Eds.), *Geochemical Processes at Mineral Surface*, vol. 323, pp. 54–78.